Stem Cell Research & Therapy

RESEARCH

Open Access

Human menstrual blood-derived stem cells secreted ECM1 directly interacts with LRP1α to ameliorate hepatic fibrosis through FoxO1 and mTOR signaling pathway

Yangxin Fang[1†], Lin Chen[1†], Yin Yuan[1], Sining Zhou[1], Jiamin Fu[1], Qi Zhang[1], Ning Zhang[1], Yuqi Huang[1], Yifei Li[1,2], Li Yuan[3], Lijun Chen[1,2*] and Charlie Xiang[1,2,4*]

Abstract

Background Human menstrual blood-derived stem cells (MenSCs), a major class of mesenchymal stem cells (MSCs), modulate intercellular signals via paracrine factors. Previous studies found that MenSC-derived secretomes exert protective effects against liver fibrosis. However, the underlying mechanisms of these observations remain unclear.

Methods Extracellular Matrix Protein 1 (ECM1), identified in MenSCs culture medium using mass spectrometry, was employed to stably overexpress ECM1-HA or silence in MenSCs using lentiviral vectors. These genetically engineered cells were either intravenously injected into the carbon tetrachloride (CCl_4)-induced liver fibrosis mice or co-cultured with hepatic stellate cells (HSCs)-LX-2. The interaction between ECM1 and low-density lipoprotein receptor-related protein 1α (LRP1α) was confirmed using Co-Immunoprecipitation (Co-ip), Duolink Proximity Ligation Assays (PLA) and pull-down. LRP1 deficient mice were generated via intravenous administration of adeno-associated-virus-8. The downstream molecular mechanisms were characterized by non-target metabolomics and multiplex immunohistochemical staining. RNA sequencing was performed to evaluate the genetic alterations in various genes within the MenSCs.

Results MenSC-secreted ECM1 exhibits potential to ameliorate liver fibrosis by inactivating HSCs, improving liver functions, and reducing collagen deposition in both cellular and mouse model of the CCl_4-induced liver fibrosis. Mechanistically, a novel interaction was identified that ECM1 directly bound to cell surface receptor LRP1α. Notably, the antifibrotic efficacy of MenSC was negated in LRP1-deficient cells and mice. Moreover, the ECM1-LRP1 axis contributed to the alleviation of liver fibrosis by suppressing AKT/mTOR while activating the FoxO1 signaling pathway, thereby facilitating pyrimidine and purine metabolism. Additionally, ECM1-modified MenSCs regulate the transcription of intrinsic cytokine genes, further mitigating liver fibrosis.

†Yangxin Fang and Lin Chen contributed equally to this work.

*Correspondence:
Lijun Chen
chenlijun@zju.edu.cn
Charlie Xiang
cxiang@zju.edu.cn

Full list of author information is available at the end of the article

Conclusions These findings highlight an extensive network of ECM1-LRP1 interaction, which serve as a link for providing promising insights into the mechanism of MenSC-based drug development for liver fibrosis. Our study also potentially presents novel avenues for clinical antifibrotic therapy.

Keywords Liver fibrosis, Hepatic stellate cells, Human menstrual blood-derived stem cells, Extracellular matrix protein 1, Low-density lipoprotein receptor-related protein 1

Background

Hepatic fibrosis is a chronic pathological process resulting from liver damage, including viral hepatitis, autoimmune and drug-induced liver disease, alcoholic steatohepatitis, and metabolic-associated fatty liver disease (MAFLD) [1, 2]. Fibrosis occurs from an excessive accumulation of extracellular matrix (ECM) within the region of the liver lesion [3]. Hepatic fibrosis could be reversed if its underlying cause is eliminated or through timely intervention [4]. Hepatic stellate cells (HSCs), situated within the space of Disse, largely synthesize massive amounts of ECM components during cell differentiation into myofibroblast-like cells in response to injury or inflammation cytokines, such as transforming growth factorβ1(TGFβ1) [5]. Furthermore, activated HSCs also secret TGFβ1, which reinforcing excessive collagen production through autocrine and paracrine loops [6]. Most studies on fibrosis focus on inhibiting the conversion of quiescent HSCs into activated HSCs to achieve an antifibrotic effect.

Extracellular matrix protein 1 (ECM1) is an 85 kDa secreted glycoprotein [7] involved in tumor metabolism and fibrosis of various organs [8–10]. In the context of liver fibrosis, Fan et al. reported that ECM1, secreted by hepatocytes, alleviated liver fibrosis through its interaction with the cell integrin αv. This interaction prevented the activation of latent transforming growth factor beta 1 (LTGFβ-1) and inhibiting HSC activation [11]. Recent studies indicate that ECM1 mediates the hepatoprotective effects by binding to proteases. ECM1 blocks LTGFβ-1 activation, achieved through binding to TSP-1 and ADAMTS1 at their respective KRFK or KTFR motifs, thereby inhibiting the activity of MMP-2/9 [12]. This protein also inhibits ferroptosis via binding to solute carrier family 7 member 11 (SLC7A11, xCT), thereby reducing liver fibrosis [13]. Moreover, ECM1 interacts with connective tissue growth factor (CTGF) to inhibit integrin αvβ6-mediated activation of TGFβ, preventing liver fibrosis and ductular reaction (DR) in alcohol-associated liver disease (ALD) and cholangiopathy [14]. Therefore, it is crucial to establish a safe and effective method to deliver ECM1 to the liver, as well as ensuring its stable and sustained expression in the liver.

Human menstrual blood-derived stem cells (MenSCs), first isolated from human menstrual fluid and named by Meng et al., are defined as a type of mesenchymal stem cells (MSC) [15]. MSC mediates antifibrotic effects via paracrine mechanisms [16]. MSCs-secreted paracrine factors, such as hepatocyte growth factor (HGF) and nerve growth factor (NGF), directly impede HSC activation by inhibiting nuclear factor-kappa B (NF-κB) signaling [17]. Milk fat globule-EGF factor 8 (MFG-E8) is an antifibrotic glycoprotein in MSC secretomes that strongly inhibits TGFβ signaling and reduces ECM deposition and liver fibrosis in mice [18]. Compared with other MSCs, MenSCs present numerous advantages, such as facile non-invasive isolation, high proliferation, and robust immunomodulatory effects on T cells [19]. Our previous studies showed that MenSCs can effectively differentiate into hepatocyte-like cells in vitro and alleviate fibrosis through immunoregulation and paracrine effects [20–22]. To date, the exact secreted proteins of MenSC that predominantly inhibit the progression of liver fibrosis remain unknown.

In the present study, we firstly identified that ECM1 functions as an antifibrotic protein in the secretomes of MenSC using mass spectrometry. We further explored the impacts and signaling mechanisms of MenSC-secreted ECM1 in vitro cell co-culture system and mice model of the carbon tetrachloride (CCl_4)-induced liver fibrosis. To this end, we constructed a protein interaction network for ECM1. Mechanistically, our investigation revealed that ECM1 directly interacted with LRP1α, mediated pyrimidine and purine metabolism, and involved in inhibiting mTOR and activating FoxO1 signaling pathways. Collectively, our results suggest that the therapeutic effect of MenSC against liver fibrosis is likely predominantly mediated by the ECM1–LRP1 axis. This comprehensive analysis underscores the antifibrotic potential of MenSC and provides new avenues for the development of liver fibrosis treatments.

Materials and methods

Mice

The study adheres to the guidelines established by the ARRIVE 2.0 checklist (Additional file 1). All Specific pathogen-free C57BL/6 male mice were purchased from SLAC Laboratory Animal Co., Ltd. (Shanghai, China). All mouse experiments were approved by the Animal Care and Use Committee of Zhejiang University (Approval no. ZJU20230279). All animals were housed in a single specific pathogen-free (SPF) room, subjected to controlled conditions of a constant temperature, 50% humidity, a 12-hour light–dark cycle, and had access to abundant

water and food to mitigate the effects of potential environmental contaminants in Laboratory Animal Center, Zhejiang University. Our pre-experimental findings indicated a statistically significant difference with a minimum sample size of six. Mice that succumbed to the experiment were excluded, and the survivors were incorporated into subsequent investigations.

C57BL/6 male mice applied in all experiments, four-week-old, 18–20 g weight, were equipped with ear tags and randomly assigned to control and carbon tetrachloride (CCl_4) (Macklin, China) model groups using Excel (Microsoft Corporation, Redmond, WA). Mice were injected intraperitoneally with CCl_4 at a concentration of 0.6 μl/g body weight dissolved in olive oil (Sangon Biotech, Shanghai, China), three times a week for 4 weeks. The control group were injected intraperitoneally with the same volume of olive oil. The dosages and method of administrating MenSCs were consistent with our previous work [20]. CCl_4-induced liver fibrosis mice which were further randomly assigned treatment groups were injected with MenSCs, ove-ECM1-HA MenSCs, sh-ECM1-MenSCs ($5 \times 10^{\wedge}5$ cells in 100 μl of PBS per mouse) or rec-ECM1 (50 μg/kg or 150 μg/kg, R&D, USA) via the tail vein twice weekly accompanied by CCl_4. Liver biopsies and serum collection were performed 3 days after the last CCl_4 administration. All mice underwent anesthesia using 1% pentobarbital prior to blood collection from the infraorbital venous plexus and liver biopsies. The mice were euthanized with CO_2 for at least 10 min after sampling. Each animal was designated as a single experimental unit. The final groups were as follows ($n = 6$): (1) control; CCl_4; CCl_4 and 50 μg/kg recombinant ECM1; CCl_4 and 150 μg/kg recombinant ECM1; (2) control; CCl_4; CCl_4 and MenSCs; CCl_4 and ove-ECM1-MenSCs; CCl_4 and ECM1-KD-MenSCs. Researchers conducting the data analysis remained blinded to the group allocations until the final statistical outcomes were obtained.

In vivo Bioluminescent assays

Mice were treated with the same ways as described. Each received an intravenous injection of $5 \times 10^{\wedge}5$ cells in 100 μl of PBS including MenSCs-luciferase (abbreviated MenSCs-luc), ove-ECM1-MenSCs-luciferase (ove-ECM1-MenSCs-luc), and ECM1-KD-MenSCs-luciferase (ECM1-KD-MenSCs-luc). Mice were intraperitoneally injected with D- luciferin (Promega, USA), and *in vivo* bioluminescence images were acquired using the IVIS Lumina LT system (Perkinelmer).

LRP1 knock down mice model

The adeno-associated virus 8 that knock down the LRP1(sh-LRP1, 5'-GGATTCCACTAGATCCCAATG-3') gene in mouse livers was constructed by Vigene Bioscience (Shandong, China). *In vivo*, the four-week-old male mice were injected intraperitoneally with 100 μl of virus containing $5 \times 10^{\wedge}11$ AAV8-shLRP1-GFP and AAV8-scramble (scr)-GFP and then treated with CCl_4 (0.6 μl /g body weight, three times a week) for another 4 weeks to establish fibrosis model. The method and dosage of MenSCs transplantation are the same as described above. The final groups were as follows ($n = 6$): control; CCl_4; CCl_4 and AAV8-scr; CCl_4, AAV8-scr and MenSCs; CCl_4 and AAV8-LRP1-KD; CCl_4, AAV8-LRP1-KD and MenSCs.

Cell culture

In this study, human MenSCs (no. 00612-210415P) were obtained from the Innovative Precision Medicine Group (IPM, Hangzhou, China). Written informed consent was obtained from the donor. The methods for the isolation, culture, and the surface marker and differentiation of identification of MenSCs were performed as previously described by our group [20, 23]. HEK293T cells (Cell Bank of Chinese Academy of Sciences, Shanghai, China) and human immortalized HSC cell line LX-2 (Procell Life Science & Technology, Wuhan, China) were cultured in DMEM (Gibco, Grand Island, NY, USA) containing 10% fetal bovine serum (FBS) (Gibco, USA) and 1% penicillin and streptomycin (Gibco, USA) at a humidified 37 °C incubator with 5% CO_2.

Plasmid construction and lentivirus packaging

The pCDH-ECM1-HA and pcDNA3.1-LRP1-Flag were obtained from GenScript (Nanjing, China) and used to overexpress ECM1 and LRP1. ShRNA sequences targeting human ECM1 (shRNA1: GCCAGAGCACTTTCAAGAAGT; shRNA2: GGCCTTCTCCAGACAATCTGA; shRNA 3: GGGAGGATACCCTTGACAAAT) were synthesized by Sangon Biotech and inserted into a pLKO.1 cloning vector to silence ECM1 expression. PCR was used to generate LRP1-Δ1(amino acids 1-1182)-Flag, LRP1-Δ2(amino acids 1183–2473)-Flag, LRP1-Δ3(amino acids 2474–3284)-Flag, LRP1-Δ4(amino acids 3285–3872)-Flag, LRP1-Δ5(amino acids 3873–4544)-Flag, Strep-LRP1-C(amino acids 2474–3872), ECM1-Δ1(amino acids 1-177)-HA, ECM1-Δ2(amino acids 178–432)-HA, ECM1-Δ3(amino acids 433–540)-HA, and ECM1-full length based on pcDNA3.1-LRP1-Flag and pCDH-ECM1-HA backbone respectively. Fragments encoding the LRP1-Flag and ECM1-HA constructs were respectively cloned into the pcDNA3.1(+) and pCDH-CMV-MCS-EF1-Puro vectors. Fragments encoding LRP1-Δ3–4 and ECM1 full length were respectively cloned into the pET-TwinStrep and pGEX-4T-1 vectors (Lingke Biotech, China). The human LRP1 guide RNA (sgRNA1: TGGAGGACAAGATCTACCGC; sgRNA2: GGAGACAGGTGAGAACCGCG; sgRNA3: CCATGCC

GAATCAACAACGG) was synthesized and cloned into the lentiCRISPR v2 vector (Lingke Biotech, China).

To obtain lentivirus, the pCDH-ECM1-HA or pCDH or pLKO.1-ECM1 or pLKO.1 or pCDH-ECM1-Δ1(amino acids 1-177)-HA or pCDH-ECM1-Δ2(amino acids 178–432)-HA or pCDH-ECM1-Δ3(amino acids 433–540)-HA or sgRNA constructs were co-transfected with packaging plasmids pSPAX2 and pMD2G into 80% confluent HEK293T cells. After 60 h transfection, viral supernatants were collected, filtered through a 0.45 μm low protein binding membrane (Millipore, Germany) and then combined with the Lenti-X Concentrator (Takara, Beijing, China) to concentrate lentiviral stocks.

Cell transfection

For transfection, pCDNA3.1-LRP1-Δ1(amino acids 1-1182)-Flag, pCDNA3.1-LRP1-Δ2(amino acids 1183–2473)-Flag, pCDNA3.1-LRP1-Δ3(amino acids 2474–3284)-Flag, pCDNA3.1-LRP1-Δ4(amino acids 3285–3872)-Flag or pCDNA3.1-LRP1-Δ5(amino acids 3873–4544)-Flag vectors were transfected into HEK293T cells using polyethyleneimines. Lentivirus supernatants were used for transduction of HEK293T, MenSCs or LX-2 cells with 8 ug/mL polybrene (Sigma, USA) for 48 h. Stable cells were selected with 1–2 μg/mL puromycin (Gibco, USA). Protein expression levels were measured by using western blotting to analyze the efficiency of overexpression, knockdown or KO.

Cell activation and co-culture

LX-2 cells were stimulated with 3 ng/ml of TGFβ1 (Peprotech, USA) for 48 h in MEM medium without FBS. After activation, LX-2 cells were treated with 100 ng/mL or 300 ng/mL rec-ECM1 for 48 h and collected for further analysis. In addition, MenSCs and activating LX-2 cells were co-cultured in six-well Transwell inserts (0.4 μm pore size, Corning, USA). MenSCs were seeded into the upper chamber at a density of $2 \times 10\hat{}5$ cells in MEM α containing 10% FBS. Respectively, the lower chambers were filled with LX-2 cells at a density of $10\hat{}5$ cells in MEM α containing 10% FBS. The co-culture system was grown in a humidified incubator at 37 °C and 5% CO_2 for 48 h. LX-2 cells in the lower chambers were collected for further analysis.

Flow cytometry

MenSCs were harvested and incubated with antibodies against surface marker and isotype control, including CD29 (BD, #561795), CD73 (BD, #561014), CD90(BD, #561970), CD105 (BD, #560839), CD34 (BD, #560941), CD45 (BD, #560975), CD117 (BD, #561682), HLA-DR (BD, #560943), IgG1 (BD, #555749), and IgG2a (BD, #555574) in the dark at 4 °C for 30 min. All MenSCs were detected using flow cytometry (CytoFLEX S, Beckman, USA).

Co-immunoprecipitation (Co-ip) and pull-down assay

Cells were lysed with Pierce IP lysates (Invitrogen, USA) containing protease and phosphatase inhibitor Cocktail (Invitrogen, USA) for 20 min on ice. The lysates were centrifuged at 12,000 ×*g* for 15 min at 4 °C. Supernatants were incubated with rotation with 25 μL of conjugated beads (anti-FLAG M2 magnetic beads (Sigma, USA) or anti-HA agarose beads (Smart-Lifesciences Biotechnology, China)) for 3 h at 4 °C or specific antibodies against endogenous protein for 2 h at 4 °C followed by the addition of protein A/G magnetic beads (Invitrogen, USA) for overnight at 4 °C. The beads were then washed three times using PBS, resuspended with 2 × SDS-PAGE loading buffer and boiled for 10 min at 100 °C. The lysates were detected using SDS-PAGE and followed by Coomassie blue staining or WB.

Pull-down assay was carried out to detect protein–protein interactions. First, GST or GST-ECM1 and TwinStrep-LRP1 proteins were purified with GST beads (Sangon Biotech, China) and TwinStrep beads (Sangon Biotech, China), respectively, from IPTG-induced BL21 bacterial cells (Sangon Biotech, China). Next, GST or GST-tagged proteins were eluted twice by reduced glutathione at 4 °C for 30 min with gentle rotation. The supernatant was collected and incubated with TwinStrep-tagged protein at 4 °C for 2 h with gentle rotation. The beads were washed three times and boiled with SDS-loading buffer. The lysates were detected by SDS-PAGE, followed by Coomassie blue staining or WB.

Mass spectrometry (MS) analysis

ECM1 and its interacting proteins were immunoprecipitated as described above for the Co-ip assay. Proteins purified by HA-Affinity beads and 200 mL of MenSC culture medium collected at above 80% cell density were subjected to LC-MS/MS analysis in Applied Protein Technology Co. Ltd (Shanghai, China). MS spectra were retrieved the UniProtKB human database using Proteome Discoverer 2.5. Candidate proteins were selected based on the number of unique peptides greater being > 2 and then analyzed using western blotting.

RNA sequencing

Total RNA was extracted from MenSCs utilizing TRIzol reagent (Invitrogen, USA). RNA quality control, cDNA library assembly, RNA sequencing, and bioinformatics analysis were conducted by Shanghai Applied Protein Technology Co., Ltd (Shanghai, China).

qRT-PCR

Total RNA was isolated from mouse liver or MenSCs using RNA extraction kit (Qiagen, USA). cDNA was synthesized using PrimeScript RT reagent (Takara, China). qRT-PCR was performed using SYBR Green PCR kit (Takara, China) and CFX96 Touch Real-Time PCR Detection System (Bio-Rad, USA). mRNA expression level was calculated using the 2^-ΔΔCt method. β-actin was used as a control. The primers used for this analysis are listed in Additional File 2 Supplementary Table S1.

Western blotting analysis

Whole cell lysates were extracted using RIPA lysis buffer (Beyotime, China) with 1% phenylmethylsulfonyl fluoride (Beyotime, China) on ice for 15 min and centrifuged at 12,000 rpm for 10 min at 4 °C. The supernatants were boiled in loading buffer (Sangon Biotech, China) for 10 min. Notably, 30 μg of total protein extracts was loaded and electrophoresed with 8% or 10% SurePAGE gels (GenScript, China) or Color PAGE Gel Rapid Preparation Kit (Epizyme Biotech, China), and then blotted onto a PVDF membrane (Millipore, USA). After blocking with 5% milk for 1 h, membranes were incubated with indicated primary antibodies at 4 °C overnight and were visualized with secondary HRP-conjugated antibodies (CST, USA). Protein bands were detected with ECL blotting detection reagents (FDbio, China) by Bio-Rad ChemiDoc Touch (Bio-Rad, USA) or Amersham ImageQuant 800 (Cytia, USA). The following primary antibodies were listed: α-SMA (1:2000, Abcam Cat# ab7817), LRP1β (1:2000, Abcam Cat# ab92544), LRP1α (1:2000, Sigma-Aldrich Cat# L2295), COL1a1(1:2000, Cell Signaling Technology Cat# 72026), ECM1 (1:2000, Sigma-Aldrich Cat# HPA027241), Flag M2 (1:2000, Sigma-Aldrich Cat# F3165), HA-Tag (1:2000, Cell Signaling Technology Cat# 3724), Fibronectin (FN) (1:2000, Cell Signaling Technology Cat# 26836), GST(1:2000, Cell Signaling Technology Cat# 2622), Strep-tag II(1:2000, Abcam Cat# ab184224), AKT(1:2000, Cell Signaling Technology Cat# 4691), p-AKT(1:2000, Cell Signaling Technology Cat# 4060), mTOR(1:2000, Cell Signaling Technology Cat# 2983), p-mTOR(1:2000, Cell Signaling Technology Cat# 5536), FoxO1(1:2000, Cell Signaling Technology Cat# 2880), β-Actin (1:5000, Cell Signaling Technology Cat# 4967) and α-Tubulin(1:5000, Cell Signaling Technology Cat# 2144).

ELISA

MenSCs were cultured in 100 mm dishes at a density of 5×10^5 cells per milliliter in MEM α supplemented 10% FBS. Upon reaching a cell density of 90%, the culture medium was replaced with serum-free MEM α for 48 h. The culture medium was then collected. We assessed the protein concentration of ECM1 in the supernatant from NC-MenSCs, ove-MenSCs and KD-MenSCs using ELISA. The ELISA was performed according to the manufacturer's protocol (Raybiotech, USA).

Proximity ligation assay

The Duolink in situ proximity ligation assay (PLA) was performed according to the manufacturer's protocol (Sigma-Aldrich, USA). Briefly, LX-2 cells were grown to a confluence of 60-70% on glass coverslips, washed three times with PBS, fixed in 4% formaldehyde for 20 min, permeabilized in 0.5% Triton X-100 for 5 min and blocked with Duolink® blocking solution for 60 min at 37 °C. After blocking, cells were incubated with primary antibodies (mouse anti-LRP1 1:500 and rabbit anti-ECM1 1:500) in the Duolink antibody diluent. The slides were then placed in the humid chamber at 4 °C overnight. Next, the slides were applied with the PLUS and MINUS PLA probe solution for 1 h at 37 °C and performed with ligation and amplification by using Duolink® In Situ Detection Reagents Red. After final Washes, the slides were mounted by using a minimal volume of Duolink® In Situ Mounting Medium with DAPI. Images were detected by a confocal microscopy and the red spots represented the interactions between ECM1 with LRP1.

Liver function

In clinical assessments, alanine aminotransferase (ALT) and aspartate aminotransferase (AST) are commonly used to assess liver function. Therefore, mouse serum was collected for the determination of ALT and AST using the ALT and AST assay kit (Jiancheng Bioengineering Institute, Nanjing, China). The optical density was detected at 410 nm using SpectraMax M5. Subsequently, the ALT and AST levels were calculated based on the standard curve according to the manufacturer's protocol.

Histological analysis

Fresh liver tissues were fixed in formalin, embedded in paraffin, and sliced. Liver tissues (3 μm thickness) were stained with hematoxylin-eosin (H&E) staining, Masson's trichrome, and SR staining. The images were examined using the Olympus digital slice scanner VS200.

Immunohistochemical and multiplex immunohistochemical staining

The paraffin-embeded liver tissues were sliced with 3 μm thickness. After deparaffinization, rehydrating, antigen retrieval, quenching and blocking, slides were incubated with primary antibody (α-SMA, GFP (HuaBio, Cat# ET1602-7)) at 4 °C overnight, applied with peroxidase conjugated secondary antibody in the diluent for 1 h at room temperature, stained with 3, 3′-diaminobenzidine reaction solution, and imaged by Olympus digital slicing scanner VS200. Multiplex immunofluorescence staining

was performed by the manufacturer's protocol (Akoya Biosciences, Japan) with the following primary antibodies: α-SMA (1:50, Abcam Cat# ab7817), p-mTOR (1:50, Abcam Cat# ab109268) and FoxO1(1:50, Cell Signaling Technology Cat# 2880). The slides were scanned using Confocal laser scanning microscope (Leica, Germany).

Non-targeted metabolomics

For non-targeted metabolomics analysis, 200 mg mouse liver tissues were added to precooled extraction buffer (methanol: acetonitrile: H_2O; 2:2:1, v/v) and sonicated at low temperature for 30 min. The mixture was then stored at -20 ℃ for 10 min before being centrifuged at 14,000 ×*g* at 4 °C for 20 min. Following centrifugation, the supernatant was vacuum-dried. Before metabolomics analysis, the samples were dissolved in 100 µL of a 1:1 (v/v) acetonitrile: water solution. An ultrahigh performance liquid chromatography system (UHPLC; Agilent 1290; Agilent, USA) coupled with a quadrupole time-of-flight mass spectrometer (ESI/Triple TOF 5600; AB Sciex, Canada) was utilized for non-targeted metabolomics analyses in Shanghai Applied Protein Technology Co., Ltd (Shanghai, China). The samples were separated by a 2.1 mm × 100 mm ACQUIY UPLC BEH Amide 1.7 µm column (waters, Ireland). Quality control (QC) samples were employed to monitor the instrument's analysis stability and repeatability.

Statistical analysis

Statistical analyses were conducted utilizing the Prism 8 software (GraphPad Software 8). Experiments were independently replicated in triplicate. Data are presented as the mean ± SEM and statistical differences between two distinct groups were assessed using the Student's t-test. $P < 0.05$ was considered to be significant.

Results

Identification of ECM1 as an antifibrotic candidate in the secretomes of MenSC

Our previous work demonstrated that the MenSCs could adhere to plastic, undergo passaging in culture medium, positively expressed CD29, CD73, CD105, and CD90, negatively expressed HLA-DR, CD117, CD34, and CD45, and differentiated into osteoblasts, chondrocytes, and adipocytes in vitro. FACS analysis revealed that the MenSCs surface marker expression was consistent with our previous work (Additional File 3 Fig. S1A).

We first attempted to explore whether MenSCs could regulate the activation of the human HSC-LX-2 induced by TGFβ1. In serum-deficient conditions, these cells highly expressed the α-SMA protein upon activation with TGFβ1, which is link to the activation of HSC. The levels of ECM-related protein, FN and collagen type I alpha 1 (COL1A1) also increased in the presence of TGFβ1. Moreover, MenSCs treatment decreased the expression levels of α-SMA, COL1A1, and FN in TGFβ1 induced LX-2 cells (Fig. 1A). Based on the paracrine effect of MenSCs, we harvested their secretomes and analyzed the ingredients using tandem mass spectrometry (MS/MS). In total, 499 secretory proteins were identified in the secretomes of MenSC (Additional File 4). Among these proteins involved in biological processes, such as ECM organization, ECM disassembly, collagen metabolic processes, and cell substrate adhesion, five candidate proteins, including MMP2, MXRA5, ECM1, LGALS3BP, and LTBP4, caught our attention due to their potential to regulate fibrosis [11, 24–27]. Among these, the enrichment of ECM1 showed the top five (Fig. 1B). Next, we used the recombinant ECM1 protein (here after abbreviated as rec-ECM1) to verify the anti-fibrotic effects *in vivo* and *in vitro*. Rec-ECM1 protein dramatically decreased α-SMA levels at cellular level in the presence of TGFβ1, independent of the concentration. Furthermore, FN and COL1A1 protein levels decreased concurrently (Fig. 1C). To explore the effects of the rec-ECM1 protein on liver fibrosis, we built a CCl_4-induced liver fibrosis mice model based on the methodology outlined in a prior study [20], followed by treatment with two different doses (50 µg/Kg or 150 µg/Kg) of rec-ECM1 administered biweekly, along with the continuous administration of CCl_4 (Additional File 3 Fig. S1B). Rec-ECM1 had no significant impact on mice body weight or liver enlargement with CCl_4-induced liver fibrosis in mice (Fig. 1D). Serum biochemical analysis exhibited no difference in AST or in ALT activities among the rec-ECM1 high-dose, rec-ECM1 low-dose, and CCl_4 groups (Fig. 1E and F). Hematoxylin and eosin (H&E) staining revealed a disordered structure of the hepatic lobule, extensive infiltration of inflammatory cells around the portal areas, and the formation of inflammatory zonules extending into the liver parenchyma. Notably, liver damage and inflammatory cell infiltration did not decrease following rec-ECM1 therapy. Masson's trichrome and Sirius red (SR) staining showed that the CCl_4 treatment caused remarkable fiber deposition in the fibrotic septa and collagen fibers that extended from the portal area in a reticular pattern compared with the control group. However, rec-ECM1 therapy did not reverse the collagen accumulation (Fig. 1G and H). Notably, activated HSCs expressed α-SMA, and CCl_4 significantly increased α-SMA expression, as revealed by IHC evaluation. However, no difference in α-SMA expression was observed between the rec-ECM1- and CCl_4-treated groups (Fig. 1I and J). Therefore, we speculated that the rec-ECM1 could directly act on LX-2 cells *in vitro* without being affected by other cell types or complex microenvironments. However, many inflammatory factors and oxidative stress, which were prevalent within the microenvironment of liver fibrosis, could significantly impact

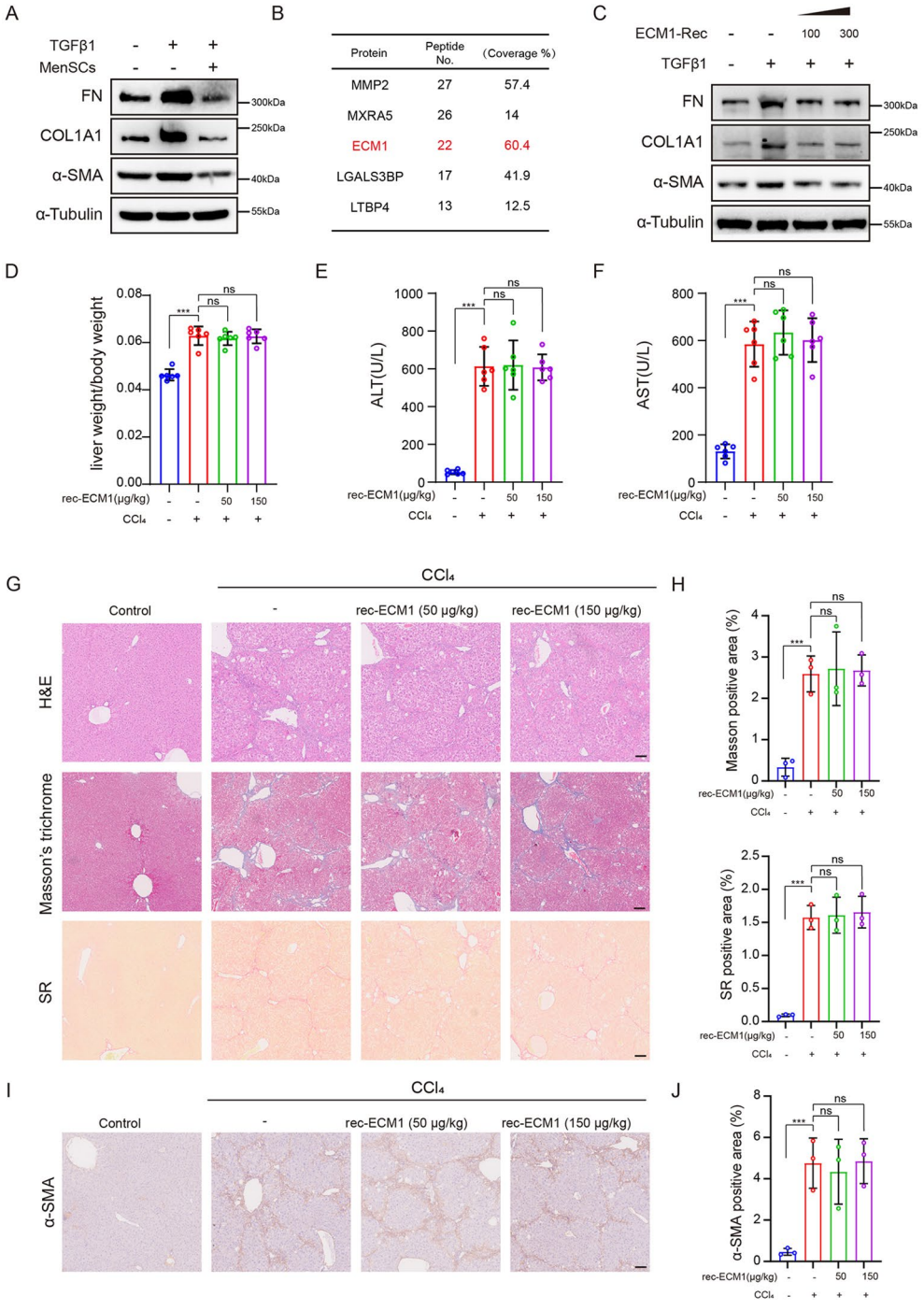

Fig. 1 Recombinant ECM1 inhibits HSC activation *in vitro* but not *in vivo*. **A** Western blotting analyses of FN, COL1A1, and α-SMA protein levels in LX-2 cells. α-Tubulin was used as loading control. Full-length blots are presented in Additional file 9. **B** Mass spectrometry analyses of MenSCs culture medium. The features of the top five protein candidates are displayed. **C** Western blotting analysis of FN, COL1A1, and α-SMA protein levels in LX-2 cells with indicated concentrations after recombinant (rec)-ECM1 treatment. α-Tubulin was used as loading control. Full-length blots are presented in Additional file 9. **D** Ratios of liver weight to body weight of control, CCl_4, and rec-ECM1-treated group. **E** and **F** Analysis of serum ALT and AST activities in control, CCl_4, and rec-ECM1-treated group. **G** H&E, Masson's trichrome, and SR staining of paraffin sections of livers from control, CCl_4, and rec-ECM1-treated group. **H** Semi-quantitative analysis of Masson's trichrome and SR staining using ImageJ from different groups. **I** α-SMA staining of paraffin sections of livers from control, CCl_4, and rec-ECM1-treated group. **J** Semi-quantitative analysis of α-SMA staining using ImageJ from different groups. Data are represented as the mean ± SEM, and three mice in each group were analyzed. Scale bar = 200 μm. ns: no sense, $^{*}P < 0.05$, $^{**}P < 0.01$, $^{***}P < 0.001$

the activity and stability of rec-ECM1. In addition, rec-ECM1 was susceptible to rapid metabolism or clearance *in vivo*, leading to a suboptimal concentration in the targets tissue, such as the liver. Collectively, rec-ECM1 could suppress HSC activation *in vitro* but did not alleviate liver fibrosis in mice.

MenSC-derived ECM1 inhibits HSC activation and alleviates liver fibrosis *in vivo* and *in vitro*

As rec-ECM1 therapy failed to alleviate liver fibrosis in mice, we used MenSCs that could home to the injured area to continuously express exogenous ECM1. First, ectopic overexpression and knockdown of ECM1 in MenSC was successfully constructed (Fig. 2A). The ECM1 protein concentration in the supernatant of NC-MenSCs, ove-MenSCs and KD-MenSCs was consistent with intracellular ECM1 protein expression levels, as confirmed by ELISA (Additional File 5 Fig. S2A). Following TGFβ1 stimulation, LX-2 cells were co-cultured with NC-MenSCs (MenSCs transfected with pLKO.1 or pCDH vectors respectively), ove-ECM1-MenSCs or ECM1-KD-MenSCs for 48 h. α-SMA, FN, and COL1A1 expression was markedly decreased in the ove-ECM1-MenSCs co-cultured group (Fig. 2B). A dramatic increase was observed in α-SMA, FN, and COL1A1 expression in the ECM1-KD-MenSCs co-cultured group compared with the NC-MenSCs (Fig. 2C). Interestingly, the ECM1-KD-MenSC co-cultured group exhibited a slightly reduced level of α-SMA, FN, and COL1A1 compared with those exposed to TGFβ1. These findings demonstrated that ove-ECM1-MenSCs were more effective than naïve MenSCs in preventing LX-2 cell activation. To address the therapeutic effect rather than the preventive effect, we injected MenSCs, ove-ECM1-MenSCs, or ECM1-KD-MenSCs into the caudal vein biweekly along with continuous CCl_4 administration (Additional File 5 Fig. S2B). In the MenSC-luc, ove-ECM1-MenSC-luc and sh-ECM1-MenSC-luc treatment models, no significant differences were observed among the cell biodistributions across these groups (Additional File 5 Fig. S2C). The finding indicated that ECM1 did not impact the distribution and migration of MenSC *in vivo*. Following transplantation with ove-ECM1-MenSCs, the mice exhibited a significant reduction in the hepatic index and serum levels of ALT and AST compared to those receiving NC-MenSCs (Fig. 2D, F, and H). Interestingly, under the same experimental conditions, the hepatic index and serum ALT and AST activity were evidently higher in mice grafted with ECM1-KD-MenSCs groups than in mice grafted with NC-MenSCs. Notably, a slight decrease was observed in the hepatic index and serum ALT and AST levels in mice grafted with ECM1-KD-MenSCs compared with those in the CCl_4 group (Fig. 2E, G, and I). Mice in the ove-ECM1-MenSCs-treated group exhibited significant reductions in inflammatory injury and collagen deposition compared with those in the NC-MenSCs-treated group. Following the ECM1-KD-MenSCs graft, mice developed worse inflammatory injury and collagen deposition in the liver than mice grafted with NC-MenSCs, as demonstrated by H&E and Masson's trichrome staining (Fig. 2J and K) and SR staining (Additional File 5 Fig. S2D and E). To further determine whether ove-ECM1-MenSCs could achieve better inhibitory effects on HSC activation, we assessed the level of α-SMA expression in the liver via IHC. We found that the ove-ECM1-MenSCs treated group exhibited a significant decrease in α-SMA expression compared with the NC-MenSCs treated group. In contrast, the expression of α-SMA was higher in mice grafted with ECM1-KD-MenSCs groups than in mice grafted with NC-MenSCs. Notably, a slight decrease was observed in α-SMA expression in mice grafted with ECM1-KD-MenSCs compared with those in mice in the CCl_4 group (Fig. 2L and M). In addition, mice in the ove-ECM1-MenSCs-treated group exhibited higher ECM1 expression levels compared to those in the NC-MenSCs-treated group. Mice in the ECM1-KD-MenSCs-treated group exhibited lower ECM1 expression levels compared to those in the NC-MenSCs-treated group (Additional File 5 Fig. S2F). These observations align with findings that demonstrate a negative correlation between ECM1 protein expression levels and the severity of liver fibrosis. Therefore, our data indicated that MenSC-secreted ECM1 inhibited HSC activation and improved liver fibrosis in mice.

ECM1 directly interacts with LRP1

We aimed to clarify the mechanisms underlying the inhibition of HSCs activation and the antifibrotic effects of ECM1 in the secretomes of MenSCs. To identify the proteins that regulate this reaction, we performed affinity purification of HA-tagged ECM1. Liquid chromatography–mass spectrometry (LC-MS/MS) analysis of this protein lysate identified LRP1 as an ECM1-interacting protein (Additional file 6, Fig. 3A). The interaction of ECM1 with LRP1 was verified using proximity ligation assay (PLA) (Fig. 3B) and reciprocal Co-ip following the overexpression of both proteins in HEK293T cells (Fig. 3C). Furthermore, an endogenous association between ECM1 and LRP1 was demonstrated in LX-2 cells. ECM1 bound to the extracellular subunit LRP1α, not LRP1β (Fig. 3D and E). To identify the binding regions of LRP1 and ECM1, we tested a series of truncation mutants for LRP1 and ECM1 in vitro binding assays (Fig. 3F and H). Notably, the ligand repeat sequence 4 of LRP1 (Fig. 3G) and the N-terminal region of ECM1 (Fig. 3I) were responsible for their interaction. PLA also revealed that the ligand repeat sequence 4 of LRP1 interacted with the N-terminal region of ECM1 (Additional

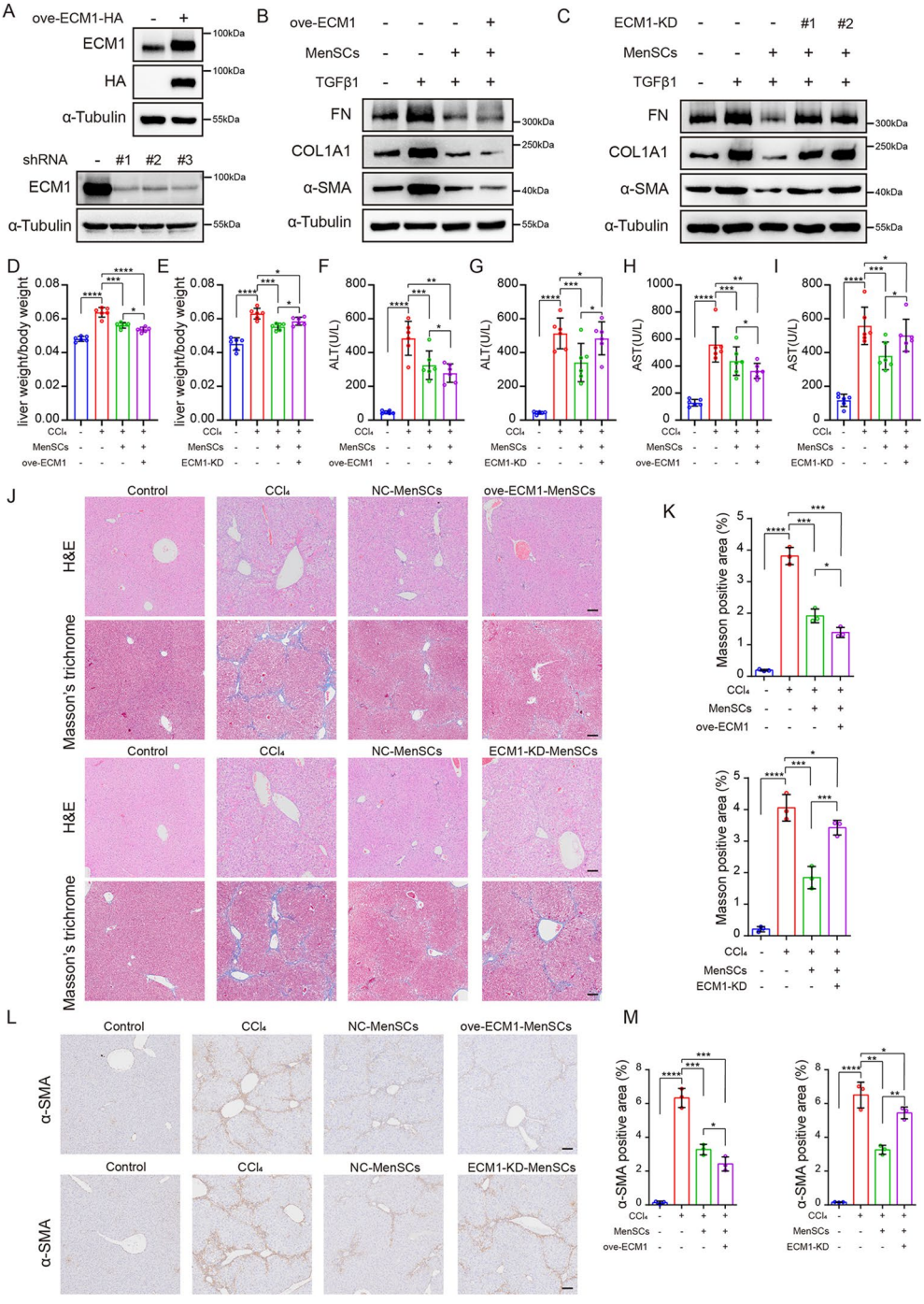

Fig. 2 MenSC-secreted ECM1 depresses HSC activation and attenuates liver fibrosis *in vivo* and *in vitro*. **A** Western blotting analyses of HA-tag and ECM1 protein levels in MenSCs after ECM1 knockdown or overexpression. α-Tubulin was used as loading control. Full-length blots are presented in Additional file 9. **B** Western blotting analyses of FN, COL1A1, and α-SMA protein levels in LX-2 cells co-cultured with NC-MenSCs or ove-ECM1-MenSCs. α-Tubulin was used as loading control. Full-length blots are presented in Additional file 9. **C** Western blotting analyses of FN, COL1A1, and α-SMA protein expression in LX-2 cells co-cultured with NC-MenSCs or ECM1-KD-MenSCs. α-Tubulin was used as loading control. Full-length blots are presented in Additional file 9. **D** Ratios of liver weight-to-body weight of control, CCl_4, NC-MenSC, and ove-ECM1-MenSC-treated group. **E** Ratios of liver weight-to-body weight of control, CCl_4, NC-MenSC and ECM1-KD-MenSC-treated group. **F** and **H** Analysis of serum ALT and AST levels from control, CCl_4, NC-MenSC, and ove-ECM1-MenSC-treated group. **G** and **I** Analysis of serum ALT and AST levels from control, CCl_4, NC-MenSC and ECM1-KD-MenSC-treated group. **J** H&E and Masson's trichrome staining of paraffin sections of livers from control, CCl_4, NC-MenSC, and ove-ECM1-MenSC or ECM1-KD-MenSC treated groups. **K** Semi-quantitative analysis of Masson's trichrome staining using ImageJ from control, CCl_4, NC-MenSC, and ove-ECM1-MenSC- or ECM1-KD-MenSC-treated groups. **L** α-SMA staining of paraffin sections of livers from control, CCl_4, NC-MenSC, and ove-ECM1-MenSC- or ECM1-KD-MenSC-treated groups. **M** Semi-quantitative analysis of α-SMA staining using ImageJ from control, CCl_4, NC-MenSC, and ove-ECM1-MenSC- or ECM1-KD-MenSC-treated groups. Data are represented as the mean ± SEM, and three mice in each group were analyzed. Scale bar = 200 μm. $^*P < 0.05$, $^{**}P < 0.01$, $^{***}P < 0.001$, $^{****}P < 0.0001$

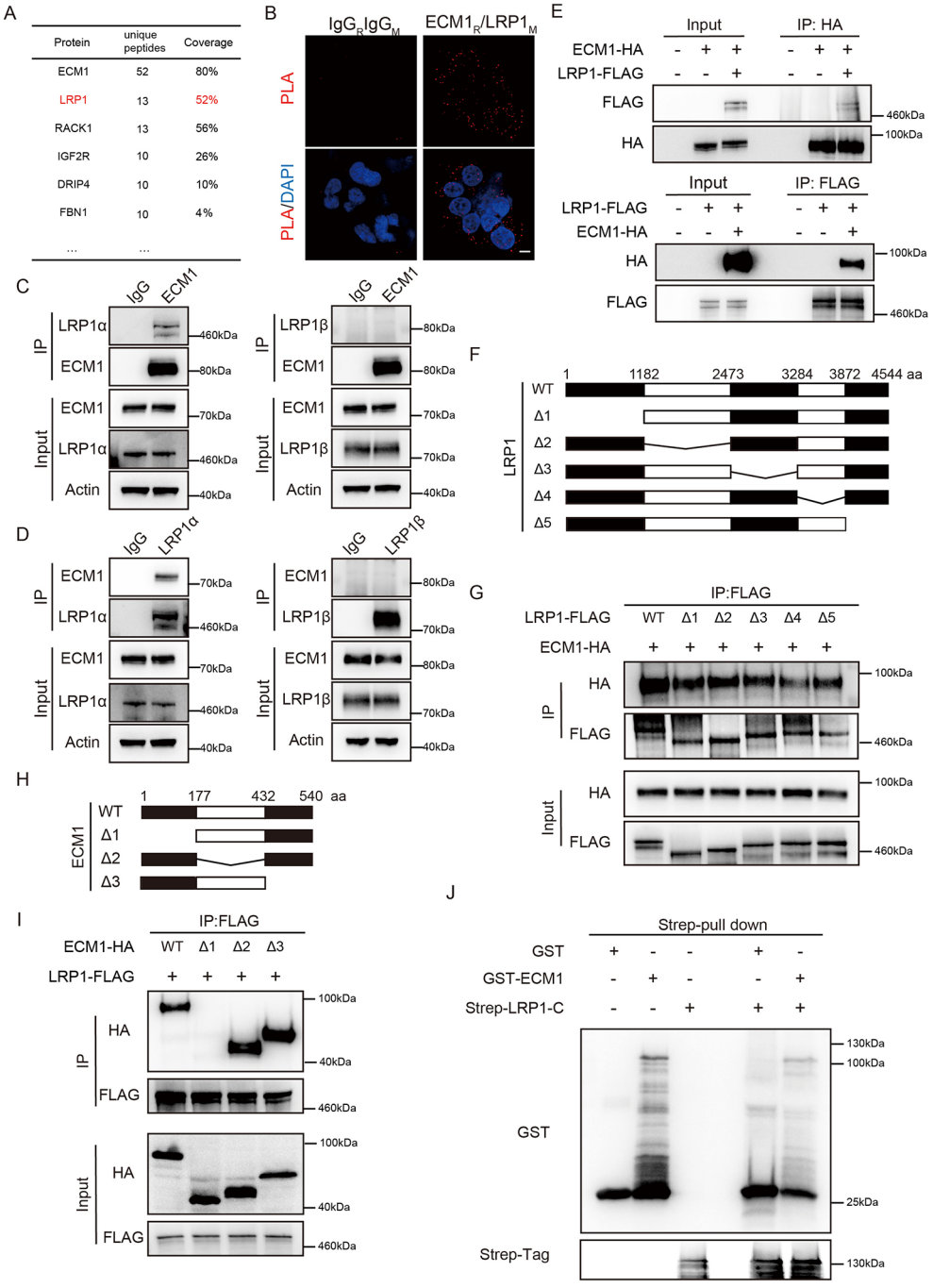

Fig. 3 ECM1 directly interacts with LRP1α. **A** Mass spectrometry analyses of proteins purified using affinity HA-tag in LX-2 cells transfected with ECM1-HA. The features of the top five protein candidates are displayed. **B** Representative duolink in situ PLA images of the interaction of ECM1 and LRP1α. PLA signals are shown in red and the nuclei in blue. Scale bar = 2 μm. **C** Co-ip in LX-2 cells. IP with ECM1 or IgG control antibody. **D** Co-ip in LX-2 cells. IP with LRP1α (left) or LRP1β (right) or IgG control antibody. **E** Reciprocal Co-ip in HEK293T cells expressing HA-tagged ECM1 and FLAG-tagged LRP1. IP with anti-HA (upper) or anti-FLAG (lower). **F** and **H** Schematics of LRP1α **F** and ECM1 **H** full length and domain deletion mutants for domain mapping assays. **G** Co-ip in HEK293T cells transfected with LRP1-FLAG deletion constructs (WT, full length; Δ1, amino acids 1–1182; Δ2, amino acids 1183–2473; Δ3, amino acids 2474–3284; Δ4, amino acids 3285–3872; Δ5, amino acids 3873–4544), and ECM1-HA. IP performed with anti-FLAG and IB with anti-HA. **I** Co-ip in HEK293T cells transfected with ECM1-HA deletion constructs (WT, full length; Δ1, amino acids 1–177; Δ2, amino acids 178–432; Δ3, amino acids 433–540), and LRP1-FLAG. IP performed with anti-FLAG and IB with anti-HA. **J***In vitro* pull-down assay of GST-ECM1 or GST alone in the presence of Strep tag-LRP1. Blots were probed for anti-GST and anti-Strep-tag. Full-length blots are presented in Additional file 9

File 7 Fig. S3A and S3B). *Invitro* pull-down assays further confirmed that LRP1 directly interacted with ECM1, as determined using western blotting (Fig. 3J) and Coomassie bright blue staining (Additional File 7 Fig. S3C). These findings illustrate that ECM1 could directly bind to LRP1α.

LRP1 is responsible for MenSC-mediated inhibition of HSC activation and alleviation of liver fibrosis

To determine whether LRP1 is the direct target of ECM1 in the secretomes of MenSCs, we constructed LRP1 knockout (KO) LX-2 cells using CRISPR CAS9 (Fig. 4A). Notably, the protein expression levels of α-SMA, FN, and COL1A1 in LRP1 KO cells were increased following TGFβ1 treatment. However, the expression levels of α-SMA, FN and COL1A1 were comparable between non-MenSCs-treated and MenSCs-treated groups following LRP1 KO. Moreover, MenSC treatment in LRP1 KO LX-2 cells increased the expression levels of α-SMA, FN and COL1A1 compared with those of MenSC treatment in wild type LX-2 cells (Fig. 4B). To demonstrate its relevance *in vivo*, mice were administrated with AAV8-shRNA-LRP1 (KD) and AAV8-scramble-LRP1 (scr) intravenously, accompanied by CCl_4-induced liver fibrosis (Fig. 4C), which resulted in the selective knockdown of LRP1 expression in the liver (Fig. 4D; Additional File 8 Fig. S4). Using this model, we observed that the hepatic injury, collagen deposition, and HSC activation worsened with the LRP1 knockdown in the liver, as demonstrated by the hepatic index (Fig. 4E), ALT and AST activities (Fig. 4F and G), H&E, Masson's trichrome staining, SR staining (Fig. 4H and I) and α-SMA expression level (Fig. 4J and K). As expected, MenSCs transplantation was insufficient for repairing liver damage and liver fibrosis in mice with selectively knocked-down LRP1 in the liver. Furthermore, no notable increase was observed in the hepatic index and serum ALT and AST activities in LRP1-KD mice compared with NC group following MenSCs administration. LRP1-KD mice in the MenSC-treated group exhibited enhanced growth with marked infiltration of inflammatory cells, collagen deposition, and α-SMA expression compared with those in the NC mice in the MenSC-treated group. These findings indicate that the therapeutic effects of MenSC on liver fibrosis depend on LRP1.

MenSC promotes pyrimidine and purine metabolism to prevent liver fibrosis

Liver fibrosis is driven by metabolic dysregulation. To investigate how MenSC-secreted ECM1 affects metabolite changes in mice livers, we compared the hepatic metabolome profiles across the control, CCl_4, NC-MenSC, ove-ECM1-MenSC, and ECM1-KD-MenSC groups. Heatmap analysis of differential metabolites revealed that the hepatic metabolome profiles were substantially altered in ove-ECM1-MenSCs- and ECM1-KD-MenSCs treated mice compared with those in MenSCs treated mice (Fig. 5A and B). In addition, a pie chart displays the chemical class of changed metabolites in the ove-ECM1-MenSC treated group and ECM1-KD-MenSC treated group compared to the MenSC only treated group (Fig. 5C). Notably, 37 and 64 significantly altered metabolites were identified in ove-ECM1-MenSC- and ECM1-KD-MenSC-treated groups, respectively. In addition, we ranked the top 11 pathways that were substantially altered in the livers of the ove-ECM1-MenSC- or ECM1-KD-MenSC-treated groups compared with those of the MenSC group using the Kyoto Encyclopedia of Genes and Genomes (KEGG) enrichment analysis such as mTOR and FoxO signaling pathways and pyrimidine and purine metabolism (Fig. 5D). Specifically, purines, such as adenosine-5′-monophosphate, and pyrimidine, such as uridine 5′-monophosphate, were markedly increased in the ove-ECM1-MenSC-treated group and conversely decreased in the ECM1-KD-MenSC-treated group compared with the MenSC group (Fig. 5E and F). The increase in uridine metabolites following MenSCs treatment suggests altered uridine catabolism, therefore, we assessed the hepatic expressions of uridine-metabolizing enzymes. The mRNA expression of *UCK* was elevated in the ove-ECM1-MenSC-treated group and decreased in the ECM1-KD-MenSC-treated group compared with that in the MenSC group (Fig. 5G). Collectively, our metabolomic data indicate that MenSC-derived ECM1 attenuates HSC activation and liver fibrosis by promoting pyrimidine and purine metabolism.

mTOR and FoxO1 signaling pathways act as downstream effectors of the ECM1-LRP1 axis

Directed by the non-target metabolisms data (Fig. 5) and the signaling pathways implicated in the abrogative effect of MenSC-secreted ECM1 on liver fibrosis, we focused on mTOR and FoxO1 signaling pathways. Therefore, to assess their roles in fibrosis alleviation via LRP1, we analyzed the expression levels of AKT, p-AKT, mTOR, p-mTOR and FoxO1 in vitro (Fig. 6A). Upon MenSCs treatment, the phosphorylation levels of AKT and mTOR were significantly suppressed in LX-2 cells, in sharp contrast to recover AKT and mTOR phosphorylation levels in LRP1 KO LX-2 cells. Additionally, Following MenSCs treatment, an increase in the expression of FoxO1 was also observed but not in LRP1 deleted cells. Multiplex immunohistochemical staining further confirmed the presence of mTOR and FoxO1 signals in murine HSCs. In the CCl_4 induced mice model, MenSCs-treated mice displayed an increase percentage of FoxO1-positive cells, co-expressed with α-SMA in murine HSCs (Fig. 6B and C). Intriguingly, FoxO1 signals were reduced in LRP1

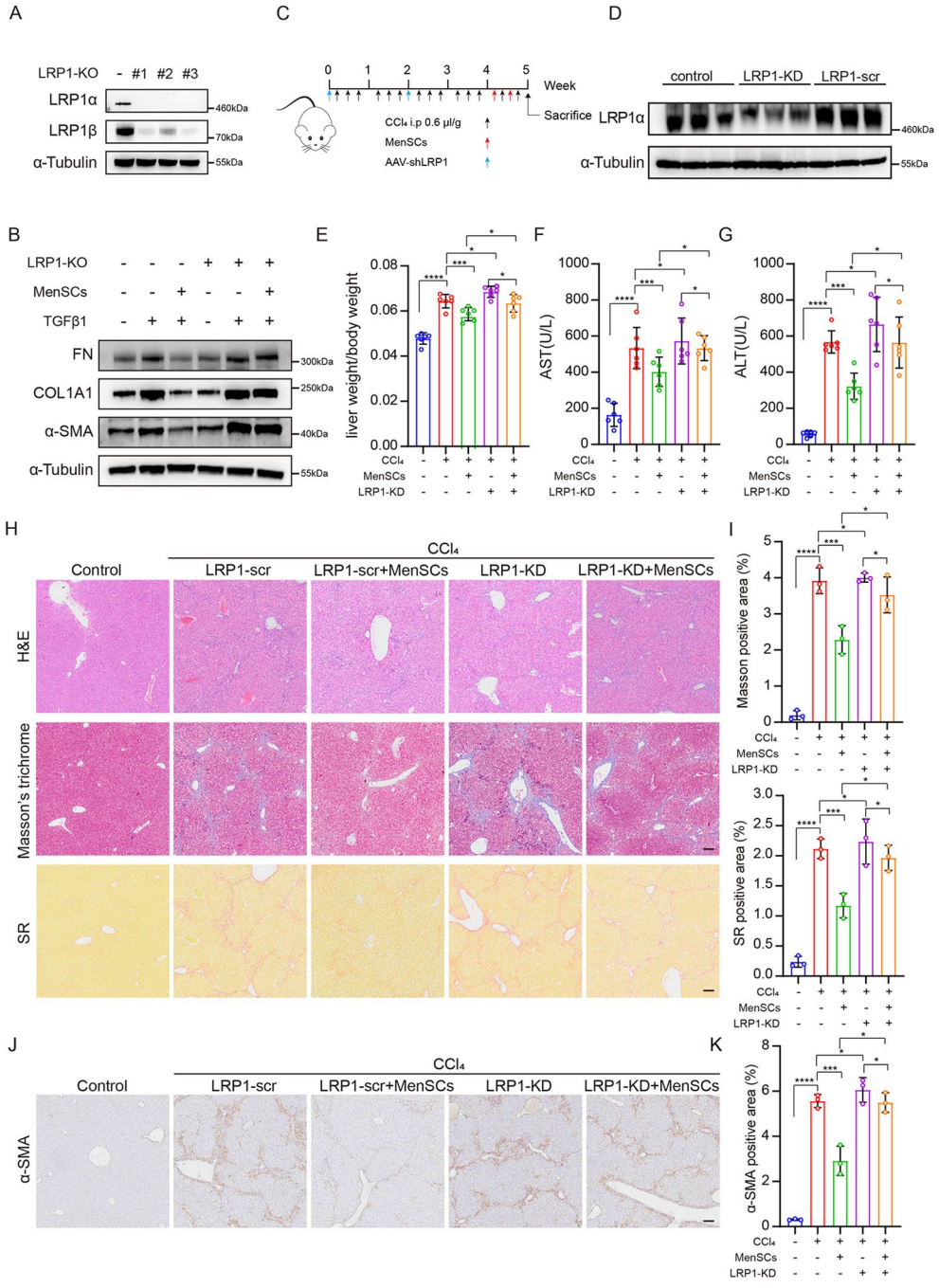

Fig. 4 LRP1 deficiency abolishes the function of MenSC during HSC inactivation and liver fibrosis alleviation. **A** Western blotting analyses of LRP1α and LRP1β protein levels in LRP1 knock out cells. α-Tubulin was used as loading control. Full-length blots are presented in Additional file 9. **B** Western blotting analyses of FN, COL1A1, and α-SMA protein levels in control or LRP1 KO cells with indicated treatment. α-Tubulin was used as loading control. Full-length blots are presented in Additional file 9. **C** Strategies of duration of shLRP1 adeno-associated virus treatment (LRP1 KD); nonsense shRNA adeno-associated virus (LRP1-scr) was used as the control group. **D** Western blotting analyses of LRP1 protein in liver tissues from control, LRP1 KD, and LRP1-scr groups. α-Tubulin was used as loading control. Full-length blots are presented in Additional file 9. **E** Ratios of liver weight-to-body weight from different groups. **F** and **G** Analysis of serum ALT and AST activities from different groups. **H** H&E, Masson's trichrome and SR staining of paraffin sections of livers from different groups. **I** Semi-quantitative analysis of Masson's trichrome and Sirius Red staining using ImageJ from different groups. **J** α-SMA staining of paraffin sections of livers from different groups. **K** Semi-quantitative analysis of α-SMA staining using ImageJ from control and the MenSC-treated group after LRP1 knockdown from different groups. Data are represented as the mean ± SEM, and three mice in each group were analyzed. Scale bar = 200 μm. **P* < 0.05, ****P* < 0.001, *****P* < 0.0001

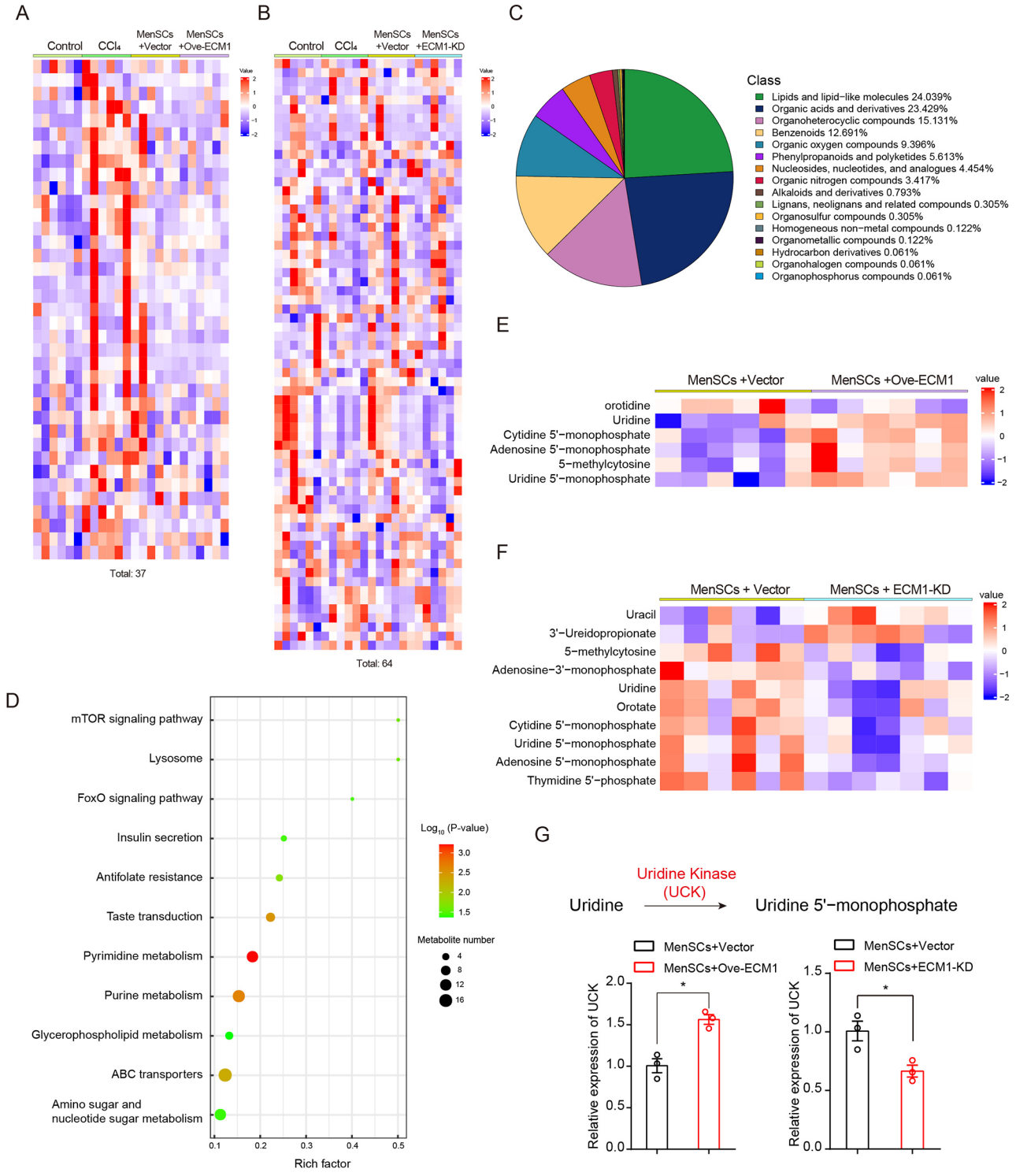

Fig. 5 Metabolome profiling of livers in MenSCs-derived ECM1 treated mice. **A** and **B** Heatmap showing differential metabolites in the liver from the ove-ECM1-MenSC- and ECM1-KD-MenSC-treated groups versus the MenSC-treated group. **C** Chemical class of changed metabolites in liver from ove-ECM1-MenSCs and ECM1-KD-MenSCs treated group compared to those from MenSCs treated group. **D** KEGG enrichment analysis of differential metabolites in the liver from the ove-ECM1-MenSC- and ECM1-KD-MenSC-treated groups compared with the MenSC-treated group. **E** and **F** Heatmap showing differential metabolites in pyrimidine and purine metabolism in the liver from the ove-ECM1-MenSC- or ECM1-KD-MenSC-treated groups compared with the MenSC-treated group. **G** Relative gene expression of UCK. β-Actin was used as loading control. *$P < 0.05$

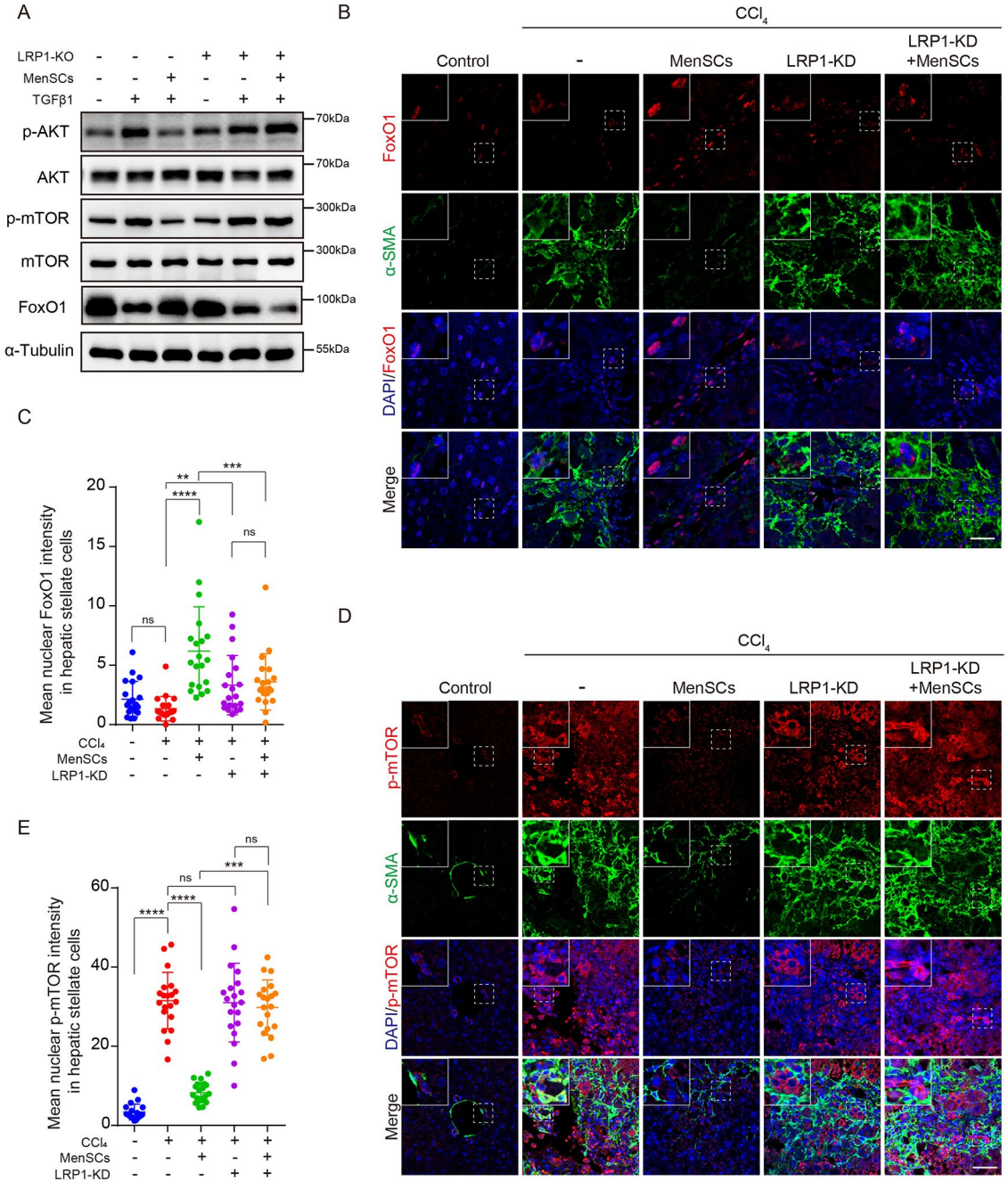

Fig. 6 ECM1-LRP1 interaction is essential for the inhibition of mTOR pathway and the activation of FoxO1 pathway. **A** Western blotting analyses of p-AKT, AKT, p-mTOR, mTOR, and FoxO1 protein levels in control or LRP1 KO cells with the indicated treatments. Full-length blots are presented in Additional file 9. **B** Representative mIHC of α-SMA and FoxO1 in liver sections from different groups. **C** Quantification of FoxO1 fluorescence intensity in the nuclei of HSCs in liver sections from different groups. $n = 20$. **D** Representative mIHC of α-SMA and p-mTOR in liver sections from different groups. **E** Quantification of p-mTOR fluorescence intensity in the nuclei of HSCs in liver sections from different groups. $n = 20$. ns: no sense, $^{**}P < 0.01$, $^{***}P < 0.001$, $^{****}P < 0.0001$

deleted livers, regardless of MenSCs treatment. These findings suggest that FoxO1 activation depends on the ECM1-LRP1 signaling axis. Moreover, we found that p-mTOR expression was downregulated in CCl_4 induced mice administrated with MenSCs (Fig. 6D and E). Conversely, p-mTOR signals remained unchanged in LRP1 depleted murine HSC, regardless of MenSCs treatment. These data suggest that both the inhibition of mTOR pathway and the activation of FoxO1 pathway both depend on ECM1-LRP1 interaction, ultimately preventing HSC activation and reducing liver fibrosis in mice.

Transcriptomic analysis reveals regulatory genes effects from ECM1-modified MenSCs

To gain insight into the potential mechanisms by which ECM1-modified MenSCs attenuate liver fibrosis independently of the ECM1–LRP1 signaling axis, transcriptomics was performed to compare changes in transcript levels. Volcano plots and fold change graphs revealed remarkably different transcriptomic profiling between MenSCs versus ove-ECM1-MenSCs and MenSCs versus shECM1-MenSCs (Fig. 7A). Heatmap analysis revealed that 12 upregulated and 7 downregulated transcripts were present in ove-ECM1-MenSCs compared with MenSCs. Furthermore, 728 upregulated transcripts and 666 downregulated transcripts were observed in

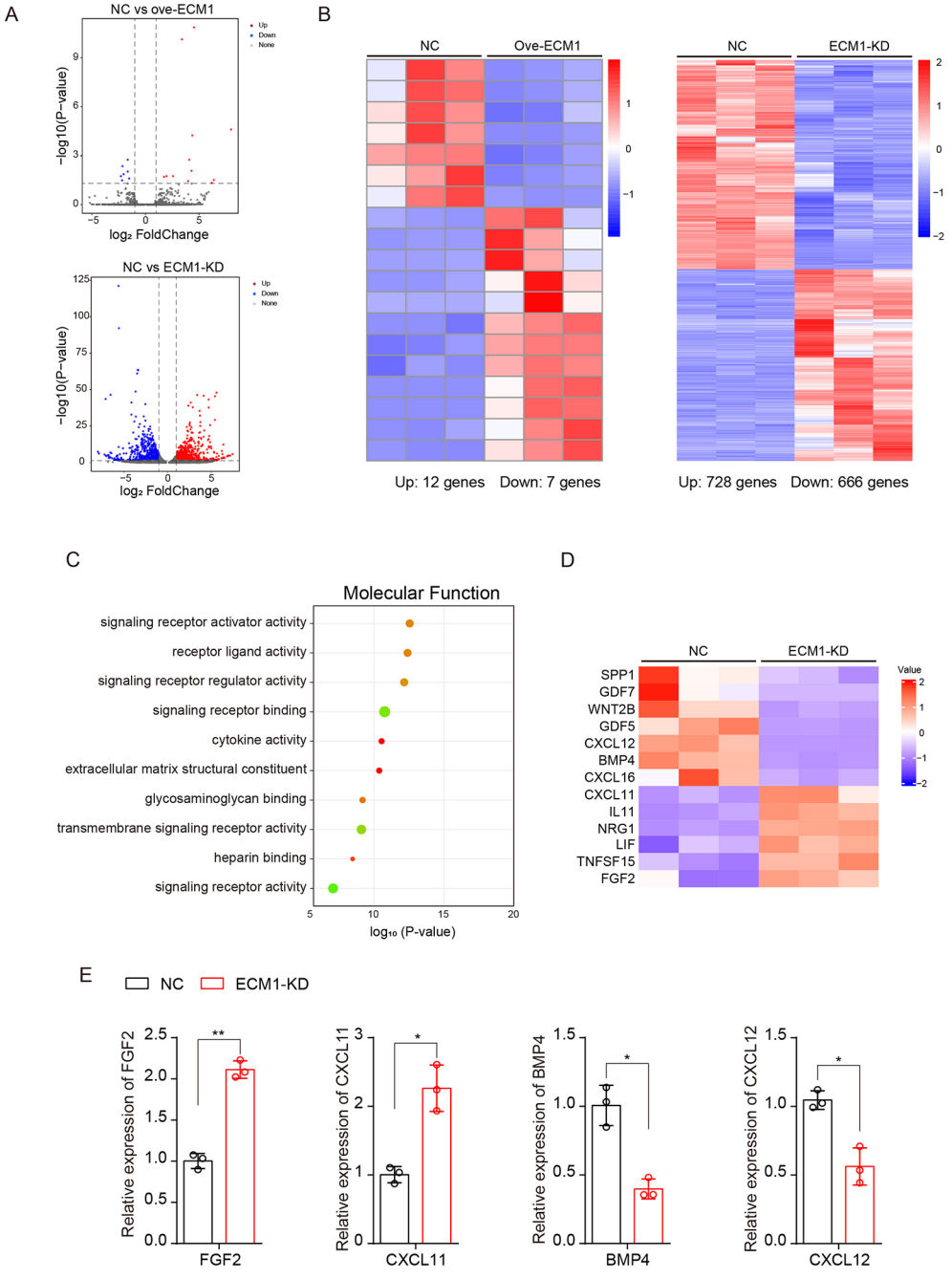

Fig. 7 Impact of ECM1 modification on the transcriptome level in MenSCs. **A** Volcano plot displaying differentially expressed genes (upregulated, red; downregulated, blue) in the ove-ECM1-MenSCs and shECM1-MenSCs compared with the MenSCs. **B** Heatmap analysis of the relative gene expression in the ove-ECM1-MenSCs and shECM1-MenSCs compared with the MenSCs. **C** KEGG analyses of differentially expressed genes in the shECM1-MenSCs compared with the MenSCs. **D** Heatmap analysis of the cytokine gene expression in the shECM1-MenSCs compared with MenSCs. **E** Relative gene expression of FGF2, CXCL11, BMP4, and CXCL12. β-Actin was used as loading control. *$P < 0.05$, **$P < 0.01$

the shECM1-MenSCs compared with those in MenSCs (Fig. 7B). Given the minor variation in ECM1 overexpressing MenSCs compared with controls, we focused on the difference between MenSCs and shECM1-MenSCs. Additionally, KEGG analysis revealed that ECM1 knockdown MenSCs improved signal receptor activator activity, receptor ligand activity, cytokine activity, and ECM structural constituents (Fig. 7C). Cytokines have been reported to be involved in HSC activation. Therefore, we analyzed cytokine transcripts in shECM1-MenSCs and compared them with those in MenSCs (Fig. 7D). Commonly downregulated cytokine genes included WNT2B and BMP4, which attenuate inflammation and fibrosis, respectively (Fig. 7D and E). Conversely, CXCL 12 and CXCL16, triggering inflammation and fibrosis, were decreased in the shECM1-MenSCs compared to those in MenSCs (Fig. 7D and E). Furthermore, upregulation of FGF2 and CXCL11 was enriched in the shECM1-MenSCs (Fig. 7D and E). Therefore, from the above observations, we hypothesize that altered cytokines in shECM1-MenSCs could contribute to HSC inactivation.

Discussion

MSC-based cell therapies have been reported to prevent the progress of hepatic fibrosis and improve liver function [28, 29]. Paracrine factors commonly play a major role in the anti-fibrotic effects of MSCs [17]. Our previous studies showed that MenSCs effectively mitigate liver fibrosis through paracrine effects [20]. Regarding the effectiveness of MSC transplantation, several alternative approaches exist beyond direct cell grafting. These include the infusion of secretomes, microvesicles derived from MSCs [18, 30], modifying gene of MSCs [31, 32] and other approaches [33]. Our *in vitro* study demonstrated that MenSCs treatment decreased the level of α-SMA, FN, and COL1A1 expression and reduced HSC activation in the presence of TGFβ1. In addition, we identified ECM1 as a candidate protein from the MenSCs culture medium to alleviate fibrosis following MenSCs transplantation. ECM1, secreted primarily by hepatocytes and HSCs and reduced in patients with chronic liver disease and even in those with stage 1–2 liver fibrosis, keeps TGFβ1 in its inactive form to prevent HSC activation and attenuate liver fibrosis [11, 12]. We recognize the necessity of developing a promising method to effectively deliver and maintain adequate therapeutic ECM1 protein expression in the liver. Various safe and efficient strategies exist for therapeutic protein delivery, such as AAV [34], extracellular contractile injection systems [35], synthetic polymers and lipid nanoparticles, and engineered extracellular vesicles [36]. Our studies revealed that rec-ECM1 administration suppressed HSC activation *in vitro* but exhibited no effect on CCl_4-induced liver fibrosis in mice. We suspected that rec-ECM1 was either inefficiently delivered to the liver injury site or was rapidly cleared or interacted with other proteins in circulation. As expected, MenSC overexpressing ECM1 enhanced the hepatoprotective effects compared with the non-manipulated MSCs in the CCl_4-induced mice liver fibrosis model. Furthermore, we found that mice transplanted with ECM1-KD-MenSCs developed worse liver fibrosis than those transplanted with MenSCs. These findings suggest that ove-ECM1-MenSCs facilitated a consistent and sustained expression of ECM1 at the site of liver injury and exerted stronger antifibrotic effect through inhibiting HSC activation than unmodified MenSCs. These observations lay the foundation for the therapeutic effect of ECM1 secreted by MenSCs on liver fibrosis. Furthermore, previous studies have shown that a gradual decrease in ECM1 expression is associated with the progression of hepatic fibrosis within the liver [11]. Complete depletion of ECM1 in mice leads to severe and spontaneous liver fibrosis [11]. ECM1 deficiency has been also implicated in the promotion of ductular reaction and liver fibrosis [14]. Conversely, ectopic overexpression of ECM1 mitigates these conditions during cholangiopathy induced by α-naphthyl-isothiocyanate (ANIT) or 3,5-diethoxycarbonyl-1,4-dihydrocollidine (DDC) and protects murine livers against alcohol-induced fibrosis [14]. However, it remains unknown whether MenSC overexpressing ECM1 exerts an antifibrotic effect in alcohol-associated liver disease or mice with ECM1 depletion in the current study.

In this study, ECM1 transmits signals to HSC through the membrane receptor, LRP1α. LRP1 is synthesized as a single 600-kDa type I transmembrane precursor. The precursor, cleaved by a furin-like convertase in the trans-Golgi network, generates an extracellular ligand-binding subunit of 515 kDa (LRP1α) and a transmembrane and intracellular subunit of 85 kDa (LRP1β) [37]. LRP-1 acts as a scavenger receptor to facilitate the endocytosis of its several ligands and as a signaling receptor to influence intracellular signal transduction [38, 39]. We found that ECM1 interacted with LRP1α, not with LRP1β at endogenous levels in LX-2 cells. LRP1α is an extracellular subunit that consists of four ligand-binding domains (DI, DII, DIII, and DIV) and repeat epidermal growth factor (EGF) [39]. Furthermore, the C-terminus of ECM1 can bind to the LG2 subdomain of the perlecan domain V, which is surrounded by EGF-like modules [40]. However, our results showed that the ligand repeat sequence 4 (amino acids 3,285-3,872) of LRP1 interacted with the N-terminal region (amino acids 1-177) of ECM1. Notably, these results differ from those of previous studies. Further elucidation of the precise molecular mechanisms is required. In addition, previous studies have shown that LRP1 can be combined with tissue plasminogen activator

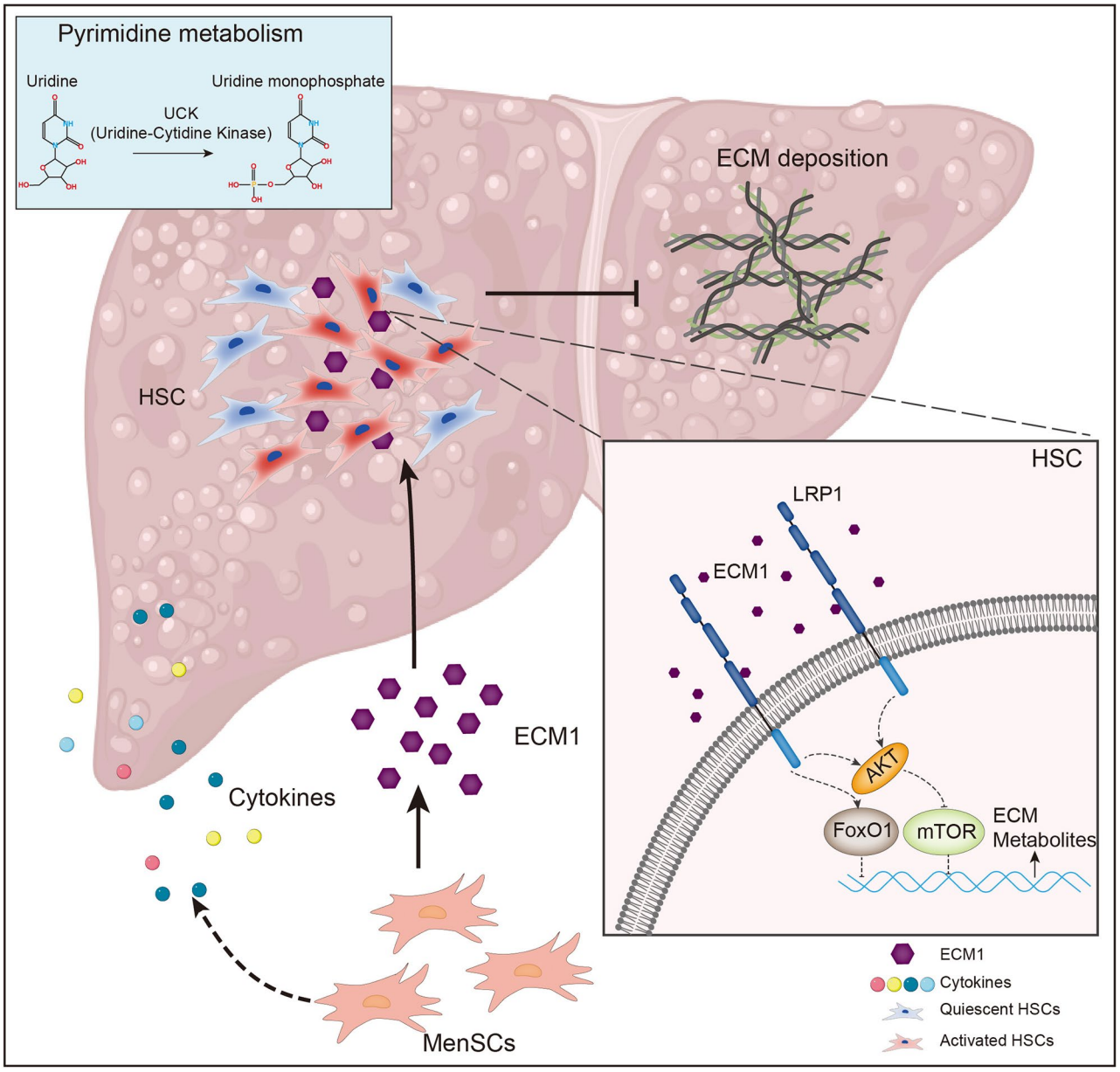

Fig. 8 Working model. ECM1 in the secretomes of MenSCs directly interacts with LRP1α through N-terminal domain and ligands repeats sequence 4 domain to subsequently suppress AKT/mTOR and activate FoxO1 signaling pathways, which promote the pyrimidine and purine metabolism and the expression of extracellular matrix, thereby inactiving HSC and ultimately attenuating liver fibrosis. Consistently, ECM1-modified MenSCs regulate the transcription of intrinsic cytokine genes to prevent liver fibrosis.

(t-PA) to promote HSC apoptosis and reverse HSC activation [41]. In our study,

we observed that MenSCs could not reverse HSC activation in LX-2 cells following LRP1 knockout and in the liver of LRP1-deficient mice. Hence, we strongly propose that LRP1 plays a vital role in mediating the effect of MenSC-derived ECM1 in inhibiting HSC activation.

The liver is crucial for regulating the body metabolism which is closely related to the development of liver fibrosis. Uridine, an essential pyrimidine nucleoside, is a key component of the nucleic acids within animal cells and participates in various metabolic processes [42]. It has been reported that uridine could alleviate CCl_4-induced liver fibrosis by attenuating hepatotoxicity and inhibiting HSC activation [43]. Our results showed an increase in pyrimidine metabolites and the accumulation of uridine in the ove-ECM1-MenSCs treated group that protected against liver fibrosis compared with those in the MenSCs treated group. These findings are consistent with previous research indicating that the inhibition of HSD17B13 can avert liver fibrosis by impeding pyrimidine catabolism in nonalcoholic steatohepatitis [44]. Additionally, it

has been demonstrated that blocking the AKT signaling pathway could delay the progression of hepatic fibrosis by diminishing ECM deposition and inhibiting HSC activation [45, 46]. We found that MenSCs reduced the expression of p-AKT and p-mTOR proteins, and increased the expression of FoxO1 in TGFβ1 induced LX-2 cells. However, the expression of p-AKT, p-mTOR and FoxO1 protein in TGFβ1 induced LRP1 knock out LX-2 cells treated with MenSCs did not change compared with those in untreated cells. In addition, we found that the expression of p-mTOR and p-FoxO1 in liver HSC was consistent with cellular results. Above all, we confirmed that ECM1 in the secretomes of MenSCs alleviates liver fibrosis and inhibits the activation of HSC through the LRP1/AKT/mTOR and LRP1/FoxO1 signaling pathways.

In this study, we observed that transplanting ECM1-KD-MenSCs did not completely eliminate the antifibrotic effect. Moreover, the inherent regulatory role of ECM1 in signal transduction of MenSCs remains poorly understood. Our transcriptomic results revealed that ECM1 knockdown in MenSCs was accompanied by the downregulation of genes that inhibit fibrosis, such as WNT2B and BMP4. Interestingly, the mRNA expressions of CXCL12 and CXCL16 were lower, while those of FGF2 and CXCL11 were higher in ECM1-KD-MenSCs than that observed in MenSCs. FGF2 and CXCL11 exhibits anti-fibrotic properties [47, 48], while CXCR4/CXCL12 and CXCR6/CXCL12 signaling can foster fibrosis [49, 50]. Beyond their paracrine effects, MenSCs contribute to liver fibrosis therapy through differentiation into hepatocyte-like cells, immunoregulatory effect and promotion of homing and engraftment [19]. However, the impact of genetically engineered ECM1-modified MenSCs on these functions remains unclear. Taken together, these results indicate that ECM1 knockdown in MenSCs is accompanied by a reduction in genes that promote fibrosis and an increase in the expression of genes that inhibit fibrosis. Therefore, ECM1 modified MenSCs attenuate liver fibrosis without affecting the ECM1-LRP1 signal axis (Fig. 8).

Conclusions

In conclusion, our findings demonstrated that ECM1, secreted by MenSCs, plays a pivotal role in the process of MenSCs-mediated liver fibrosis alleviation. The ove-ECM1-MenSCs exhibited a superior therapeutic effect on liver fibrosis compared to naïve MenSCs. Detailed data revealed that ECM1 directly interacted with LRP1α, leading to the regulation of pyrimidine and purine metabolites through inhibiting AKT/mTOR and activating FoxO1 signaling pathways. Additionally, we demonstrated that cytokine production, serving as an intrinsic regulatory factor in MenSC-mediated signal transduction to attenuate liver fibrosis beyond the ECM1-LRP1 axis. Our study provides compelling evidence of the direct interaction between ECM1 in MenSC secretomes and LRP1α, the HSC receptor, and indicates the potential of ECM1-engineered MenSCs for the targeted treatment of liver fibrosis.

Abbreviations

MenSC	Menstrual blood-derived Stem Cell
ECM1	Extracellular matrix protein 1
LRP1	Low-density lipoprotein receptor-related protein 1
HSC	Hepatic stellate cell
TGFβ1	Transforming growth factorβ1
ECM	Extracellular matrix
KD	Knock-down
Ove	Overexpression
Scr	Scramble
Luc	Luciferase
Rec	Recombination
CCl_4	Carbon tetrachloride
WT	Wild type
α-SMA	Alpha-Smooth Muscle Actin
FN	Fibronectin
COL1A1	Collagen type I alpha 1
Co-ip	Co-immunoprecipitation
PLA	Proximity Ligation Assay
Coip-MS	Co-immunoprecipitation Mass Spectrum
AAV8	Adeno-associated virus8
AST	Aspartate aminotransferase
ALT	Alanine aminotransferase

Supplementary Information

The online version contains supplementary material available at https://doi.org/10.1186/s13287-025-04351-0.

Additional file 1 The ARRIVE guidelines 2.0: author checklist

Additional file 2 Table S1 Realtime PCR primer

Additional file 3 Figure S1. Verification of MenSCs and Scheme of mice fibrosis model

Additional file 4 Complete protein identification list for MenSCs culture medium by MS, related to Figure 1B

Additional file 5 Figure S2. MenSC-secreted ECM1 depresses HSC activation and attenuates liver fibrosis ***in vivo*** and ***in vitro***

Additional file 6 Complete protein identification list for proteins purified using affinity ECM1-HA tag in LX-2 cells by IP-MS, related to Figure 3A

Additional file 7 Figure S3. ECM1 directly interacts with LRP1α

Additional file 8 Figure S4. GFP labeled adeno-associated virus expresses in murine liver cells

Additional file 9 Full-length blots/gels

Acknowledgements

Authors thank Qiong Huang, Jingyao Chen, Chao Bi and Jiajia Wang from the Core Facilities, Zhejiang University School of Medicine for their technical support.

Authors' contributions

YXF, LC, LJC, and CX conceived the study. YXF and LC conducted experiments, analyzed the data and drafted the work. LJC and CX provided suggestions. YY, SNZ, QZ, NZ, JMF, YQH, LY, and YFL provided technical assistance in some experiments. YXF, LJC, and CX substantively revised the manuscript.

Funding

This work was supported by the Zhejiang Provincial Natural Science Foundation of China (LTGY24H030002), the National Key R&D Program of China (2022YFA1105603 and 2022YFC2304405), the Fundamental Research

Funds for the Central Universities (2025ZFJH03 and 2022ZFJH003), the Zhejiang Provincial Key Research and Development Program (2019C03015), and the Shandong Provincial Laboratory Project (SYS202202).

Data availability

All data in this study are displayed in the text or Supplementary files. The raw data of RNA-sequencing has been deposited in the NCBI Sequence Read Archive (SRA) database (Accession Number: PRJNA1199730). The mass spectrometry metabolomics data have been deposited in the OMIX, China National Center for Bioinformation with the dataset identifier OMIX008343.

Declarations

Ethics approval and consent to participate

The animal experiments were approved by the Animal Care and Use Committee of Zhejiang University on Dec.04, 2023 (Approval no. ZJU20230279). Human MenSCs (no. 00612-210415P), provided by the Innovative Precision Medicine Group (Hangzhou, China). The Innovative Precision Medicine Group has confirmed that there was initial ethical approval for collection of human cells. And the donor has signed written informed consent.

Consent for publication

Not applicable.

Declaration of generative AI and AI-assisted technologies in the writing process

The authors employed ChatGPT to refine language quality and readability during the manuscript preparation.

Competing interests

Li Yuan is employee of the Innovative Precision Medicine (IPM) Group. The other authors declare that they have no competing interests.

Author details

[1]State Key Laboratory for Diagnosis and Treatment of Infectious Diseases, National Clinical Research Center for Infectious Diseases, National Medical Center for Infectious Diseases, Collaborative Innovation Center for Diagnosis and Treatment of Infectious Diseases, The First Affiliated Hospital, Zhejiang University School of Medicine, Hangzhou, Zhejiang 310003, China
[2]Research Units of Infectious Disease and Microecology, Chinese Academy of Medical Sciences, Beijing 100730, China
[3]Innovative Precision Medicine (IPM) Group, Hangzhou, Zhejiang 311215, China
[4]Jinan Microecological Biomedicine Shandong Laboratory, Jinan, Shandong 250117, China

Received: 12 December 2024 / Accepted: 17 April 2025
Published online: 07 May 2025

References

1. Hammerich L, Tacke F. Hepatic inflammatory responses in liver fibrosis. Nat Rev Gastroenterol Hepatol. 2023;20(10):633–46. https://doi.org/10.1038/s41575-023-00807-x.
2. Eslam M, Sanyal AJ, George J. MAFLD: A Consensus-Driven proposed nomenclature for metabolic associated fatty liver disease. Gastroenterology. 2020;158(7):1999–e20141. https://doi.org/10.1053/j.gastro.2019.11.312.
3. Schuppan D, Afdhal NH. Liver cirrhosis. Lancet. 2008;371(9615):838–51. https://doi.org/10.1016/s0140-6736(08)60383-9.
4. Bataller R, Brenner DA. Liver fibrosis. J Clin Investig. 2005;115(2):209–18. https://doi.org/10.1172/jci24282.
5. Lackner C, Tiniakos D. Fibrosis and alcohol-related liver disease. J Hepatol. 2019;70(2):294–304. https://doi.org/10.1016/j.jhep.2018.12.003.
6. Bissell DM, Wang SS, Jarnagin WR, Roll FJ. Cell-specific expression of transforming growth factor-beta in rat liver. Evidence for autocrine regulation of hepatocyte proliferation. J Clin Investig. 1995;96(1):447–55. https://doi.org/10.1172/jci118055.
7. Smits P, Ni J, Feng P, Wauters J, Van Hul W, Boutaibi ME, Dillon PJ, Merregaert J. The human extracellular matrix gene 1 (ECM1): genomic structure, cDNA cloning, expression pattern, and chromosomal localization. Genomics. 1997;45(3):487–95. https://doi.org/10.1006/geno.1997.4918.
8. Al Shareef Z, Kardooni H, Murillo-Garzón V, Domenici G, Stylianakis E, Steel JH, Rabano M, Gorroño-Etxebarria I, Zabalza I, Vivanco MD, Waxman J, Kypta RM. Protective effect of stromal Dickkopf-3 in prostate cancer: opposing roles for TGFBI and ECM-1. Oncogene. 2018;37(39):5305–24. https://doi.org/10.1038/s41388-018-0294-0.
9. Li Y, Fan W, Link F, Wang S, Dooley S. Transforming growth factor B latency: A mechanism of cytokine storage and signalling regulation in liver homeostasis and disease. JHEP Reports: Innov Hepatol. 2022;4(2):100397. https://doi.org/10.1016/j.jhepr.2021.100397.
10. Yin H, Wang J, Li H, Yu Y, Wang X, Lu L, Lv C, Chang B, Jin W, Guo W, Ren C, Yang G. Extracellular matrix protein-1 secretory isoform promotes ovarian cancer through increasing alternative mRNA splicing and stemness. Nat Commun. 2021;12(1):4230. https://doi.org/10.1038/s41467-021-24315-1.
11. Fan W, Liu T, Chen W, Hammad S, Longerich T, Hausser I, Fu Y, Li N, He Y, Liu C, Zhang Y, Lian Q, Zhao X, Yan C, Li L, Yi C, Ling Z, Ma L, Zhao X, Xu H, Wang P, Cong M, You H, Liu Z, Wang Y, Chen J, Li D, Hui L, Dooley S, Hou J, Jia J, Sun B. ECM1 prevents activation of transforming growth factor B, hepatic stellate cells, and fibrogenesis in mice. Gastroenterology. 2019;157(5):1352–67. https://doi.org/10.1053/j.gastro.2019.07.036.
12. Link F, Li Y, Zhao J, Munker S, Fan W, Nwosu ZC, Yao Y, Wang S, Huang C, Liebe R, Hammad S, Liu H, Shao C, Gao C, Sun B, Török NJ, Ding H, Ebert MP, Weng H, Ten Dijke P, Drasdo D, Dooley S, Wang S. ECM1 attenuates hepatic fibrosis by interfering with mediators of latent TGF-β1 activation. Gut. 2024. https://doi.org/10.1136/gutjnl-2024-333213.
13. Fu Y, Zhou X, Wang L, Fan W, Gao S, Zhang D, Ling Z, Zhang Y, Ma L, Bai F, Chen J, Sun B, Liu P. Salvianolic acid B attenuates liver fibrosis by targeting Ecm1 and inhibiting hepatocyte ferroptosis. Redox Biol. 2024;69:103029. https://doi.org/10.1016/j.redox.2024.103029.
14. Sun C, Fan W, Basha S, Tian T, Jin-Smith B, Barkin J, Xie H, Zhou J, Yin XM, Ling C, Sun B, Petersen B, Pi L. Extracellular matrix protein 1 binds to connective tissue growth factor against liver fibrosis and ductular reaction. Hepatol Commun. 2024;8(11). https://doi.org/10.1097/hc9.0000000000000564.
15. Meng X, Ichim TE, Zhong J, Rogers A, Yin Z, Jackson J, Wang H, Ge W, Bogin V, Chan KW, Thébaud B, Riordan NH. Endometrial regenerative cells: a novel stem cell population. J Translational Med. 2007;5:57. https://doi.org/10.1186/1479-5876-5-57.
16. Higashi T, Friedman SL, Hoshida Y. Hepatic stellate cells as key target in liver fibrosis. Adv Drug Deliv Rev. 2017;121:27–42. https://doi.org/10.1016/j.addr.2017.05.007.
17. Lee C, Kim M, Han J, Yoon M, Jung Y. Mesenchymal stem cells influence activation of hepatic stellate cells, and constitute a promising therapy for liver fibrosis. Biomedicines. 2021;9(11). https://doi.org/10.3390/biomedicines9111598.
18. An SY, Jang YJ, Lim HJ, Han J, Lee J, Lee G, Park JY, Park SY, Kim JH, Do BR, Han C, Park HK, Kim OH, Song MJ, Kim SJ, Kim JH. Milk fat Globule-EGF factor 8, secreted by mesenchymal stem cells, protects against liver fibrosis in mice. Gastroenterology. 2017;152(5):1174–86. https://doi.org/10.1053/j.gastro.2016.12.003.
19. Chen L, Qu J, Cheng T, Chen X, Xiang C. Menstrual blood-derived stem cells: toward therapeutic mechanisms, novel strategies, and future perspectives in the treatment of diseases. Stem Cell Res Ther. 2019;10(1):406. https://doi.org/10.1186/s13287-019-1503-7.
20. Chen L, Zhang C, Chen L, Wang X, Xiang B, Wu X, Guo Y, Mou X, Yuan L, Chen B, Wang J, Xiang C. Human menstrual Blood-Derived stem cells ameliorate liver fibrosis in mice by targeting hepatic stellate cells via paracrine mediators. Stem Cells Translational Med. 2017;6(1):272–84. https://doi.org/10.5966/sctm.2015-0265.
21. Mou XZ, Lin J, Chen JY, Li YF, Wu XX, Xiang BY, Li CY, Ma JM, Xiang C. Menstrual blood-derived mesenchymal stem cells differentiate into functional hepatocyte-like cells. J Zhejiang Univ Sci B. 2013;14(11):961–72. https://doi.org/10.1631/jzus.B1300081.
22. Chen L, Huang Y, Zhang N, Qu J, Fang Y, Fu J, Yuan Y, Zhang Q, Li H, Wen Z, Yuan L, Chen L, Xu Z, Li Y, Yan H, Izawa H, Li L, Xiang C. Single-cell RNA sequencing reveals reduced intercellular adhesion molecule crosstalk between activated hepatic stellate cells and neutrophils alleviating liver fibrosis in hepatitis B virus Transgenic mice post menstrual blood-derived mesenchymal stem cell transplantation. MedComm. 2024;5(8):e654. https://doi.org/10.1002/mco2.654.

23. Chen X, Wu Y, Wang Y, Chen L, Zheng W, Zhou S, Xu H, Li Y, Yuan L, Xiang C. Human menstrual blood-derived stem cells mitigate bleomycin-induced pulmonary fibrosis through anti-apoptosis and anti-inflammatory effects. Stem Cell Res Ther. 2020;11(1):477. https://doi.org/10.1186/s13287-020-01926-x.
24. Du Z, Lin Z, Wang Z, Liu D, Tian D, Xia L. SPOCK1 overexpression induced by platelet-derived growth factor-BB promotes hepatic stellate cell activation and liver fibrosis through the integrin α5β1/PI3K/Akt signaling pathway. Lab Invest. 2020;100(8):1042–56. https://doi.org/10.1038/s41374-020-0425-4.
25. Poveda J, Sanz AB, Fernandez-Fernandez B, Carrasco S, Ruiz-Ortega M, Cannata-Ortiz P, Ortiz A, Sanchez-Niño MD. MXRA5 is a TGF-β1-regulated human protein with anti-inflammatory and anti-fibrotic properties. J Cell Mol Med. 2017;21(1):154–64. https://doi.org/10.1111/jcmm.12953.
26. Stampolidis P, Ullrich A, Iacobelli S. LGALS3BP, lectin galactoside-binding soluble 3 binding protein, promotes oncogenic cellular events impeded by antibody intervention. Oncogene. 2015;34(1):39–52. https://doi.org/10.1038/onc.2013.548.
27. Su CT, Urban Z. LTBP4 in health and disease. Genes. 2021;12(6). https://doi.org/10.3390/genes12060795.
28. Yang X, Li Q, Liu W, Zong C, Wei L, Shi Y, Han Z. Mesenchymal stromal cells in hepatic fibrosis/cirrhosis: from pathogenesis to treatment. Cell Mol Immunol. 2023;20(6):583–99. https://doi.org/10.1038/s41423-023-00983-5.
29. Feng X, Feng B, Zhou J, Yang J, Pan Q, Yu J, Shang D, Li L, Cao H. Mesenchymal stem cells alleviate mouse liver fibrosis by inhibiting pathogenic function of intrahepatic B cells. Hepatology (Baltimore, Md). 2025;81(4):1211-27. https://doi.org/10.1097/hep.0000000000000831
30. Lou G, Chen Z, Zheng M, Liu Y. Mesenchymal stem cell-derived exosomes as a new therapeutic strategy for liver diseases. Exp Mol Med. 2017;49(6):e346. https://doi.org/10.1038/emm.2017.63.
31. Liu Q, Lv C, Huang Q, Zhao L, Sun X, Ning D, Liu J, Jiang Y, Jin S. ECM1 modified HF-MSCs targeting HSC attenuate liver cirrhosis by inhibiting the TGF-β/Smad signaling pathway. Cell Death Discovery. 2022;8(1):51. https://doi.org/10.1038/s41420-022-00846-4.
32. Hwang BW, Kim SJ, Park KM, Kim H, Yeom J, Yang JA, Jeong H, Jung H, Kim K, Sung YC, Hahn SK. Genetically engineered mesenchymal stem cell therapy using self-assembling supramolecular hydrogels. J Controlled Release: Official J Controlled Release Soc. 2015;220(Pt A):119–29. https://doi.org/10.1016/j.jconrel.2015.10.034.
33. Shi Q, Xia Y, Wu M, Pan Y, Wu S, Lin J, Kong Y, Yu Z, Zan X, Liu P, Xia J. Mi-BMSCs alleviate inflammation and fibrosis in CCl(4)-and TAA-induced liver cirrhosis by inhibiting TGF-β/Smad signaling. Mater Today Bio. 2024;25:100958. https://doi.org/10.1016/j.mtbio.2024.100958.
34. George LA, Monahan PE, Eyster ME, Sullivan SK, Ragni MV, Croteau SE, Rasko JEJ, Recht M, Samelson-Jones BJ, MacDougall A, Jaworski K, Noble R, Curran M, Kuranda K, Mingozzi F, Chang T, Reape KZ, Anguela XM, High KA. Multiyear factor VIII expression after AAV gene transfer for hemophilia A. N Engl J Med. 2021;385(21):1961–73. https://doi.org/10.1056/NEJMoa2104205.
35. Kreitz J, Friedrich MJ, Guru A, Lash B, Saito M, Macrae RK, Zhang F. Programmable protein delivery with a bacterial contractile injection system. Nature. 2023;616(7956):357–64. https://doi.org/10.1038/s41586-023-05870-7.
36. Ma D, Xie A, Lv J, Min X, Zhang X, Zhou Q, Gao D, Wang E, Gao L, Cheng L, Liu S. Engineered extracellular vesicles enable high-efficient delivery of intracellular therapeutic proteins. Protein Cell. 2024;15(10):724–43. https://doi.org/10.1093/procel/pwae015.
37. Selvais C, D'Auria L, Tyteca D, Perrot G, Lemoine P, Troeberg L, Dedieu S, Noël A, Nagase H, Henriet P, Courtoy PJ, Marbaix E, Emonard H. Cell cholesterol modulates metalloproteinase-dependent shedding of low-density lipoprotein receptor-related protein-1 (LRP-1) and clearance function. FASEB Journal: Official Publication Federation Am Soc Experimental Biology. 2011;25(8):2770–81. https://doi.org/10.1096/fj.10-169508.
38. Herz J, Strickland DK. LRP: a multifunctional scavenger and signaling receptor. J Clin Investig. 2001;108(6):779–84. https://doi.org/10.1172/jci13992.
39. Boucher P, Herz J. Signaling through LRP1: protection from atherosclerosis and beyond. Biochem Pharmacol. 2011;81(1):1–5. https://doi.org/10.1016/j.bcp.2010.09.018.
40. Mongiat M, Fu J, Oldershaw R, Greenhalgh R, Gown AM, Iozzo RV. Perlecan protein core interacts with extracellular matrix protein 1 (ECM1), a glycoprotein involved in bone formation and angiogenesis. J Biol Chem. 2003;278(19):17491–9. https://doi.org/10.1074/jbc.M210529200.
41. Kang LI, Isse K, Koral K, Bowen WC, Muratoglu S, Strickland DK, Michalopoulos GK, Mars WM. Tissue-type plasminogen activator suppresses activated stellate cells through low-density lipoprotein receptor-related protein 1. Laboratory investigation; a journal of technical methods and pathology. 2015;95(10):1117–29.https://doi.org/10.1038/labinvest.2015.94
42. Kypson J, Hait G. Effects of uridine and inosine on glucose metabolism in skeletal muscle and activated lipolysis in adipose tissue. J Pharmacol Exp Ther. 1976;199(3):565–74.
43. Zheng WV, Li Y, Cheng X, Xu Y, Zhou T, Li D, Xiong Y, Wang S, Chen Z. Uridine alleviates carbon tetrachloride-induced liver fibrosis by regulating the activity of liver-related cells. J Cell Mol Med. 2022;26(3):840–54. https://doi.org/10.1111/jcmm.17131.
44. Luukkonen PK, Sakuma I, Gaspar RC, Mooring M, Nasiri A, Kahn M, Zhang XM, Zhang D, Sammalkorpi H, Penttilä AK, Orho-Melander M, Arola J, Juuti A, Zhang X, Yimlamai D, Yki-Järvinen H, Petersen KF, Shulman GI. Inhibition of HSD17B13 protects against liver fibrosis by Inhibition of pyrimidine catabolism in nonalcoholic steatohepatitis. Proc Natl Acad Sci USA. 2023;120(4):e2217543120. https://doi.org/10.1073/pnas.2217543120.
45. Son G, Hines IN, Lindquist J, Schrum LW, Rippe RA. Inhibition of phosphatidylinositol 3-kinase signaling in hepatic stellate cells blocks the progression of hepatic fibrosis. Hepatology (Baltimore MD). 2009;50(5):1512–23. https://doi.org/10.1002/hep.23186.
46. Pan Q, Gao M, Kim D, Ai W, Yang W, Jiang W, Brashear W, Dai Y, Li S, Sun Y, Qi Y, Guo S. Hepatocyte FoxO1 deficiency protects from liver fibrosis via reducing inflammation and TGF-β1-mediated HSC activation. Cell Mol Gastroenterol Hepatol. 2024;17(1):41–58. https://doi.org/10.1016/j.jcmgh.2023.08.013.
47. Kurniawan DW, Booijink R, Pater L, Wols I, Vrynas A, Storm G, Prakash J, Bansal R. Fibroblast growth factor 2 conjugated superparamagnetic iron oxide nanoparticles (FGF2-SPIONs) ameliorate hepatic stellate cells activation in vitro and acute liver injury in vivo. J Controlled Release: Official J Controlled Release Soc. 2020;328:640–52. https://doi.org/10.1016/j.jconrel.2020.09.041.
48. Yu X, Chen Y, Cui L, Yang K, Wang X, Lei L, Zhang Y, Kong X, Lao W, Li Z, Liu Y, Li Y, Bi C, Wu C, Zhai A. CXCL8, CXCL9, CXCL10, and CXCL11 as biomarkers of liver injury caused by chronic hepatitis B. Front Microbiol. 2022;13:1052917. https://doi.org/10.3389/fmicb.2022.1052917.
49. Hong F, Tuyama A, Lee TF, Loke J, Agarwal R, Cheng X, Garg A, Fiel MI, Schwartz M, Walewski J, Branch A, Schecter AD, Bansal MB. Hepatic stellate cells express functional CXCR4: role in stromal cell-derived factor-1alpha-mediated stellate cell activation. Hepatology (Baltimore MD). 2009;49(6):2055–67. https://doi.org/10.1002/hep.22890.
50. Ma Z, Ma C, Zhang Q, Bai Y, Mu K, Liu X, Yang Q. Role of CXCL16 in BLM-induced epithelial-mesenchymal transition in human A549 cells. Respir Res. 2021;22(1):42. https://doi.org/10.1186/s12931-021-01646-7.

Publisher's note